

CHAPTER XX

ATTRIBUTION OF CLIMATE CHANGE IN THE PRESENCE OF INTERNAL VARIABILITY

John M. Wallace¹, Clara Deser², Brian V. Smoliak¹, and Adam S. Phillips²

¹*Department of Atmospheric Sciences, University of Washington,
Seattle, WA 98195, USA*

²*Climate and Global Dynamics Division, National Center for Atmospheric Research,
Boulder, CO 80305, USA*

Spontaneous, internally-generated variability of the climate system is pervasive. On the multidecadal time scale it dominates the variability of surface air temperature averaged over extratropical land areas as large as the contiguous United States, and it modulates the rate of rise of global mean temperature in response to the buildup of greenhouse gases. Unforced variability is one of the factors that imposes limitations on the degree of confidence that can be attached to assessments and predictions of human-induced climate change. This chapter summarizes results of some recent studies based on the analysis of large ensembles of numerical integrations run with a suite of different atmospheric initial conditions but with the same prescribed external forcing scenario. The future trajectory of the real climate system is, in some sense, like the trajectory of an individual member of such an ensemble. The diversity of the trends among the different ensemble members is a part of the irreducible uncertainty inherent in projections of future climate change. It is shown how statistical methods can be used to diagnose the causes of this diversity, most of which is in response to member-to-member diversity in the atmospheric circulation trends, as reflected in the associated patterns of the sea-level pressure trends. Interactions between the atmosphere, oceans, and land also contribute to the variability of surface air temperature trends on the multidecadal time scale, as discussed in Chapters XX and XX. It is argued that in the face of such large uncertainties in the attribution of climate change in the extratropics, more attention should be focused on climate change in the tropics, where the greenhouse warming signal stands out more clearly, and on the broader suite of environmental issues that impact food security and the viability of ecosystems.

1. Introduction

Many questions concerning the nature and causes of climate variability on the multidecadal time scale are still unresolved. For example, there is no consensus within the scientific community as to whether time-varying forcing associated with aerosols or whether a strengthening of the Atlantic Meridional Over-

turning Circulation was mainly responsible for the mid-20th century hiatus and the recent slowdown in the rate of global warming. Nor is it clear why the Arctic has experienced rapid warming during the past decade while surface air temperatures over the Northern Hemisphere as a whole warmed less than in the two prior decades, or why wintertime temperatures

over the Northern Hemisphere continents poleward of 40°N warmed three times as rapidly as global-mean (land plus ocean) annual-mean surface air temperature during the late 20th century (e.g., see Trenberth et al. 2007). These large spatial and temporal differences in the rate of warming stem from the fact that the climate system is varying on the multidecadal time scale in response to its own internal variability as well as to a variety of natural and anthropogenic forcings. It is often difficult to distinguish between internally generated low frequency climate variability and human-induced climate change. In the words of the Technical Summary of the IPCC’s Fourth Assessment Report, “Difficulties remain in attributing temperature changes at smaller than continental scales and over time scales less than 50 years.” (Solomon et al. 2007). These ambiguities can be expected to persist until the signature of human-induced climate change becomes large enough to stand out clearly above the natural “background variability”, as is projected to occur in the second half of this century (Deser et al. 2012a).

The causes of surface air temperature (SAT) trends over the continents can be formally separated into the four categories listed in Fig. 1, which are arranged in the form of a 2 x 2 matrix, the columns separating thermodynamically- versus dynamically-induced SAT variability and the rows separating forced versus free variability. In this terminology, *thermodynamically-induced* refers to SAT changes induced by time-varying radiative fluxes or by time-varying fluxes of sensible and latent heat at the Earth’s surface, exclusive of any concomitant changes in the atmospheric circulation and *dynamically-induced* denotes SAT changes attributable to changes in the atmospheric circulation, irrespective of their cause.

The term *forced* refers to responses to externally imposed changes in the Earth’s energy balance, including both anthropogenic influences and natural forcings such as volcanic eruptions, solar variability and, on long time scales, orbital changes. Forced, thermodynamically-induced trends in global-mean temperature (the upper left box in Fig. 1) plays a central role in projections of human-induced climate change. However, for attribution of regional and perhaps even global climate trends on the multidecadal time scale, the other three categories need to be considered as well.

If the global atmospheric circulation changes systematically in response to human-induced global warming or due to natural causes it will result in further SAT changes that can be said to be dynamically-induced (the upper right box in Fig. 1). Examples of dynamically-induced climate change include a circulation-induced poleward amplification of the temperature trend at the Earth’s surface (Alekseev et al. 2005), a widening of the tropical Hadley cells (Lu et al. 2007), a poleward shifting of the extratropical storm tracks (Yin 2005), and a systematic weakening of the tropical circulations (Vecchi and Soden 2007). It has been proposed that the “robust response to global warming” includes a suite of circula-

	thermodynamically induced	dynamically induced
Forced <small>anthropogenic and natural</small>		
Free		

FIG. 1. A scheme for categorizing the factors that contribute to trends in regional surface air temperature. See text for explanation.

tion-related changes that can be inferred from basic conservation laws (Held and Soden 2006). Other examples of externally forced dynamical responses include changes in the wintertime circulation over high northern latitudes induced by large volcanic eruptions (Robock and Mao 1994; Shindell et al. 2001) and changes in the monsoon circulations in response to the changing meridional profile of insolation induced by orbital changes (Kutzbach 1981).

Spontaneously occurring changes in the amplitude and polarity of preferred atmospheric circulation patterns such as the Northern and Southern Hemisphere annular modes (Wallace and Thompson 2002) or the patterns observed in association with ENSO (Nitta and Yamada 1989; Trenberth and Hurrell 1994; Zhang et al. 1997), as represented by the lower right box in Fig. 1, should induce regional SAT trends on the multidecadal time scale. The amplitude of the dynamically-induced SAT changes tend to be much larger over land than over sea, because of its lower heat capacity. Hence, if the dynamically-induced SAT trends project strongly upon the land-sea distribution, they may contribute to the hemispherically or globally averaged temperature trend; e.g., if they were to change in a manner so as to cool the oceans and warm the land, that would constitute a positive contribution. Dynamically-induced warming in response to atmospheric circulation changes has been invoked to account for the rapidity of the wintertime warming over Eurasia and North America poleward of 40°N during the late 20th Century (Hurrell 1996; Wallace et al. 1995, 1996; Bracco et al. 2004).

In most of the existing literature on the impacts of the unforced (or internal) variability of the climate system it is assumed that the

associated regional or global temperature trends over land are mediated by changes in the atmospheric circulation. However, it is also possible that a component of the SAT trends could be thermodynamically-induced (the lower left box in Fig. 1). For example, it has been suggested that the ENSO cycle affects SAT not only through planetary-scale teleconnections (the lower right box), but also by modulating the surface energy fluxes over the equatorial Pacific cold tongue region (Yuleva et al. 1994; Chiang and Sobel 2002). It has recently been proposed the sea surface temperature variations over high latitudes of the Atlantic Ocean and the Arctic Ocean that occur in association with unforced variations in the intensity of the meridional overturning circulation on the multidecadal time scale might be capable of causing even larger SAT variations over Eurasia on the multidecadal time scale (Semenov et al. 2010).

In the world of models, the distinctions between the four boxes are clear, at least in principle. Anthropogenically-forced climate change can be distinguished from internally generated, free climate variability based on a suite of simulations, performed with a single model in which each ensemble member is started from a different set of initial conditions and run with the same prescribed, time-varying external forcings. In principle, the trends in the ensemble-mean of the simulations can be identified with the externally forced climate change “signal” and the departures of the trends in the individual realizations from the ensemble mean trends are attributable to the internal variability of the simulated climate system. This methodology is useful when the number of individual realizations is large enough to ensure a high level of statistical significance. However, thus far, en-

sembles sizes in the CMIP simulations have been so small that it has been necessary to use multi-model ensemble means to obtain statistically significant results, in which case internal variability and model-to-model differences both contribute to the departures of the trends in the individual realizations from the ensemble-mean trend, rendering attribution problematic. In principle, thermodynamically versus dynamically forced variability can likewise be distinguished through experimentation with climate models, but in practice the design of experiments that permit one kind of forcing but not the other is not straightforward.

Just how applicable the results derived from the model world are to the real world depends upon how well the models run with and without various prescribed external forcings are able to simulate the internally generated low frequency variability of the climate system. With only one observed climate trajectory that can be used as a basis for validating the models, this question can only be addressed in a probabilistic way. Validating climate models requires a robust characterization of the low frequency variability in the historical climate record, including temporal means, variance and covariance statistics, and spectra. To obtain robust estimates of these quantities (*i.e.*, estimates with a sufficient number of statistical degrees of freedom) it is necessary to restrict the analysis to frequencies at least an order of magnitude higher than one cycle over the length of the ~ 100 -year-long historical record, *e.g.*, by applying a high pass filter. Attribution of variability with frequencies lower than this cutoff frequency is inherently ambiguous. Multidecadal variability falls within this “twilight zone” in which attribution can be performed only in a probabilistic way.

Another factor that limits our ability to diagnose the decadal-scale variability in the climate record is the fact that inherently stochastic variability on the interannual time scale associated, for example, with the ENSO cycle or with large excursions of the Northern and Southern Hemisphere annular modes is capable of inducing substantial sampling variability on the multidecadal time scale. For example, it has been questioned whether the so-called Pacific Decadal Oscillation (PDO: Mantua et al. 1997), which is alleged to be a multidecadal phenomenon is merely a manifestation of such stochastic, sampling variability (Newman et al. 2003).

Regardless of the mechanisms that give rise to it, multidecadal climate variability mediates the rate of rise of global-mean temperature. Performing a “dynamical adjustment” to remove, or at least reduce the contribution of these circulation changes that contribute to or detract from the rate of rise in global-mean temperature simplifies the space-time structure of the surface air temperature record and renders it more spatially and seasonally coherent (Wallace et al. 1995; Thompson et al. 2009).

The existence of internally generated sampling variability is well known and is discussed extensively in reviews of Barnett et al. (2005) and Hegerl et al. (2007) and the references therein. Various approaches have been used to estimate the uncertainty in past and projected SAT trends that is attributable to such “climate noise,” but the emphasis in these studies has generally been on establishing the statistical significance of historical or projected climate trends rather than on the characteristics of the noise itself. In many studies the noise is represented as formless error bars flanking the observed, reconstructed, or projected “signal.” In reality, climate noise exhib-

its distinctive space-time structure that can mimic that of human-induced climate change. Later in this chapter we will recall two relatively recent instances in which apparent secular trends deemed as having been beyond the range of natural variability have subsequently reversed, suggesting that they were, in fact, internally generated.

In this chapter we will summarize the state of our knowledge of internally generated interdecadal variability of the climate system. In the next section we will show how the interplay between free and forced climate variability complicates the attribution of global warming and regional climate impacts. In Section 3 we show examples of the dynamical contribution to SAT trends and we demonstrate how performing a dynamical adjustment can simplify the representation of climate change in the historical record. In Section 4 we offer a few brief comments relating to the internally generated thermodynamically-induced variability. In the final section we summarize and discuss the implications of these results more generally.

2. On the role of internally-generated climate variability in climate change

In this section we will discuss the role of internally-generated climate variability in climate change on space scales ranging from regional to global. We will begin in Section 2.1 by considering the diversity and spatial patterns of surface air temperature (SAT), sea level pressure (SLP) and precipitation trends in a 40 member ensemble of simulations run

with Version 3 of the Community Climate System Model (CCSM3) forced with the A1B greenhouse gas scenario initialized in 2000 and integrated forward in time through 2060. Details of the model simulations may be found in Deser et al. (2012a). Then in Section 2.2 we will show and discuss observations and simulations of global warming during the 20th Century. In interpreting these results it should be noted that existing climate models exhibit substantial diversity with respect to their mean climates and the level of internally generated climate variability. Hence, the results presented here, which are derived from only two of these models, should be regarded as illustrative, but not necessarily representative of the behavior of the real climate system.

2.1. Insights derived from projections of future trends

As background for the discussion in this subsection we show in Fig. 2a,c the ensemble mean of the 56 year (2005–2060) December–February (DJF) SLP and SAT trends in the 40 member CCSM3 ensemble in raw (hPa per 56 years; °C per 56 years) and standardized form (Fig. 2b,d respectively). The SLP trends in the ensemble mean map range up to several hPa (*e.g.*, off the west coast of Canada) but with the exception of a few patches in the tropics, they are generally much less than one standard deviation and therefore may be interpreted as sampling fluctuations. In contrast, the ensemble mean SAT trend (Fig. 2d) exhibits a robust global warming signal, with an average warming of 2–3 standard deviations over the

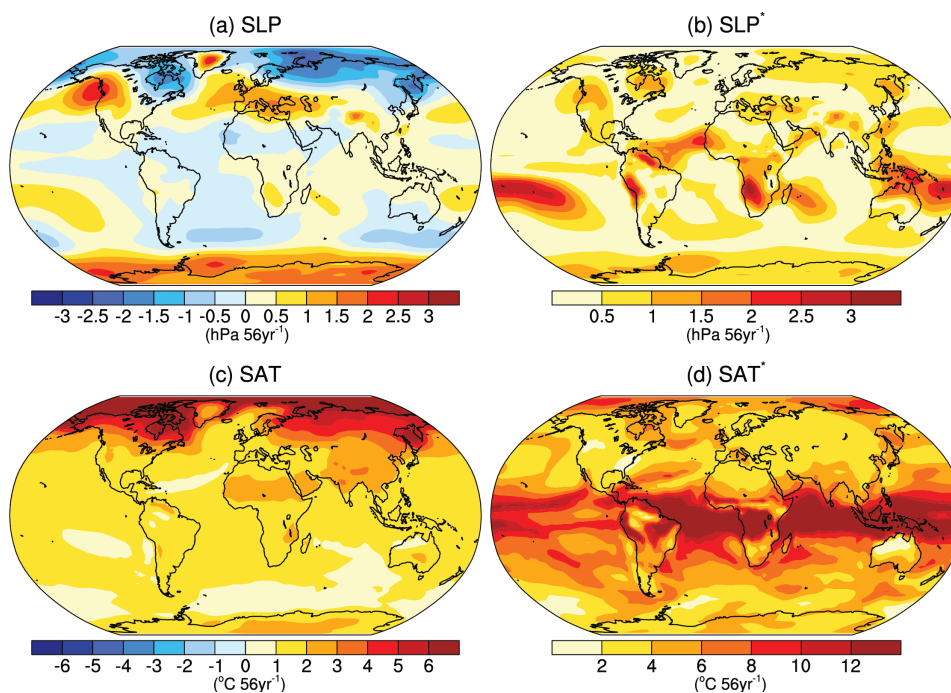


Fig. 2. DJF sea level pressure (SLP) and surface air temperature (SAT) trends for 2005-2060 in a 40-member ensemble of simulations with the CCSM3 climate model. Left panels (a) Ensemble-mean SLP trend; (b) Ensemble-mean SAT trend. Right panels (c) Standardized ensemble-mean SLP trend (SLP*) computed by dividing the ensemble mean trend at each grid point by the standard deviation of the 40-member ensemble trends at the same grid point and (d) Standardized ensemble-mean SAT trend (SAT*). From Deser et al. (2012a).

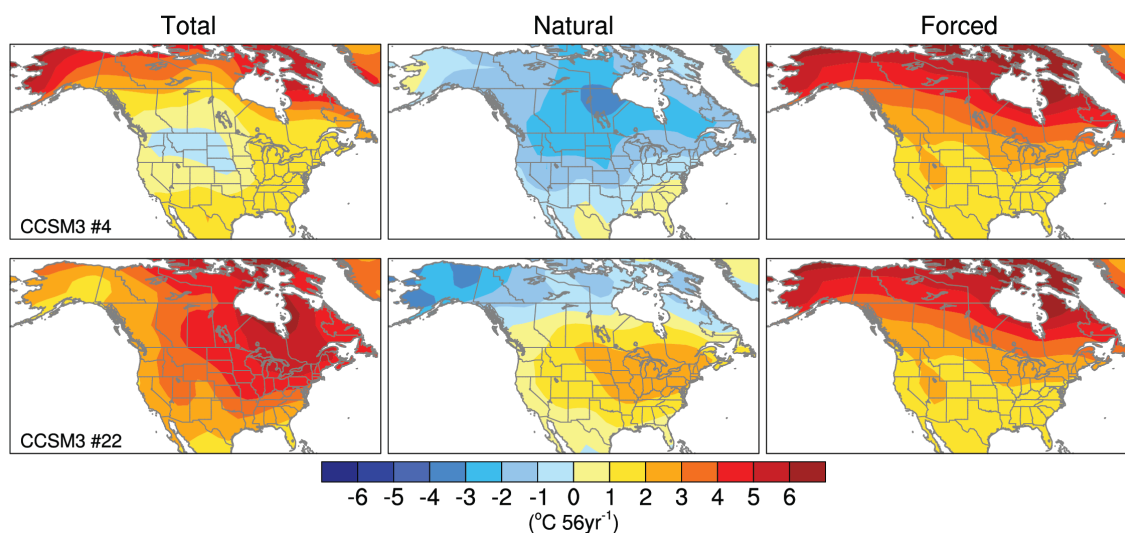


FIG. 3. Partitioning of the 56-year temperature trends in Ensemble Members #4 and #22 into a component forced by the buildup of greenhouse gases and a residual trend attributable to internally generated variability. Adapted from Deser et al. (2013).

Northern Hemisphere continents. In agreement with observations, the “signal to noise ratio” of the warming trend is larger in the tropics than at higher latitudes (Mahlstein et al. 2011, 2012).

The diversity of the patterns in SAT trends in the 40 individual ensemble members is illustrated by contrasting the 2005–2060 trends in Members #4 and #22, which correspond to the weakest and strongest warming trends averaged over the contiguous United States. In Fig. 3 the trends for these two ensemble mem-

bers are partitioned into “Forced” and “Natural” components, the former defined by the ensemble mean trend and the latter by the departure of the trends in these two ensemble members from the ensemble mean trend. It is evident that the “Natural” component of the trend, which is attributable to internally generated variability, is as large as the “Forced” component.

Figure 4 shows selected time series of SAT in Ensemble Members #4 and #22. The global-mean SAT trend (land areas only) is quite

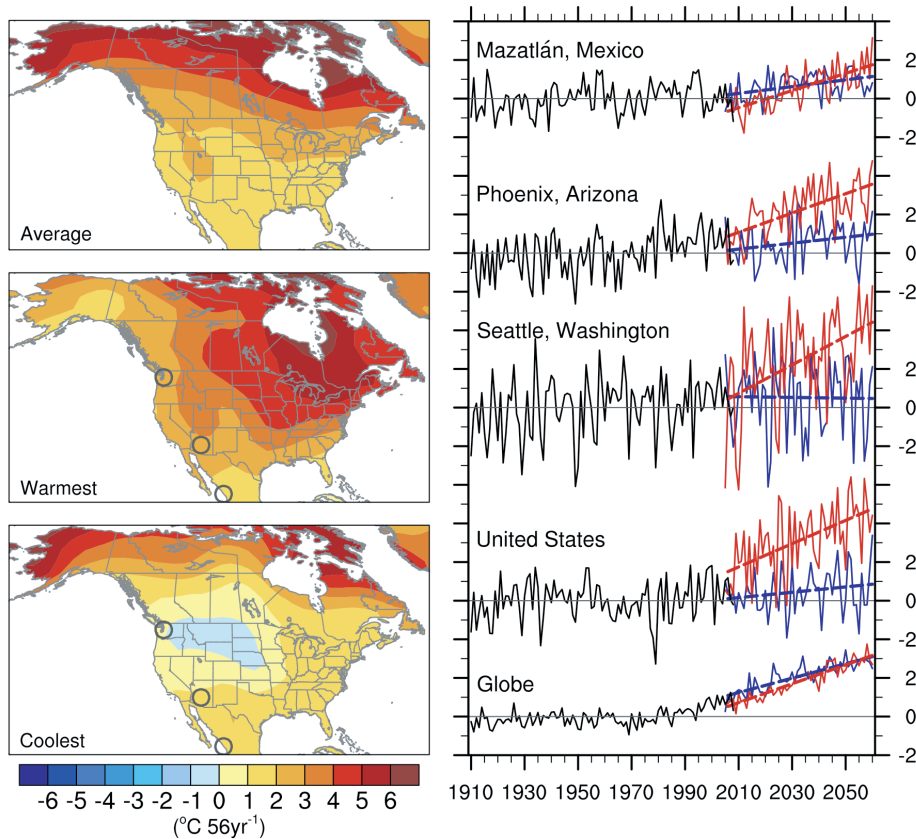


FIG. 4. (Left panels) DJF temperature trends during 2005–2060 ($^{\circ}\text{C}$ per 56 years). Top panel shows the 40-member ensemble mean; middle and bottom panels show the corresponding trends in Members #4 and #22. Right panels show DJF time series for selected regions and specific locations as indicated by the labeling and marked by the open circles in the left panels). The black segments of the curves show observed records from 1910–2008 (minus the long-term mean); the red and blue segments show model projections for 2005–2060 based on the ensemble members with the largest and smallest projected trends, respectively, for each region or location. Dashed red and blue lines show the best-fit linear trends in these same ensemble members. For visual clarity, time mean SAT in the model projections are adjusted to match to observations averaged over their common period of record 2005–2008. From Deser et al. (2012b).

comparable in the two ensemble members but the regional and local trends over the contiguous United States (CONUS) have a profoundly different character. In Member #22 average warming over the CONUS over the 56 year period is $\sim 3^\circ\text{C}$, whereas in Member #4 it is only $\sim 1^\circ\text{C}$ and cooling occurs over parts of the Pacific Northwest and the northern Rockies.

The patterns shown in Figs. 2–4 are for the boreal winter season December through February (DJF) when the internally generated variability is greatest. However, the spatial patterns in individual members of the CCSM3 40-member ensemble also exhibit substantial diversity during the boreal summer June–August (JJA), as shown in Fig. 5. The con-

trasts between outliers are not as large as during winter but they are still appreciable.

In the summertime precipitation trends based on the same 40-member ensemble, most ensemble members exhibit positive trends over Canada and Alaska, but a wide member-to-member diversity of the rainfall trends over the continental United States. The two examples shown in Fig. 6 portray sharply contrasting future rainfall trends over the Great Plains and Midwest relative to the 2005–2008 rainfall climatology in that ensemble member. Large ensembles are required to detect statistically significant precipitation trends in simulations with climate models and there is no guarantee that nature will conform to the en-

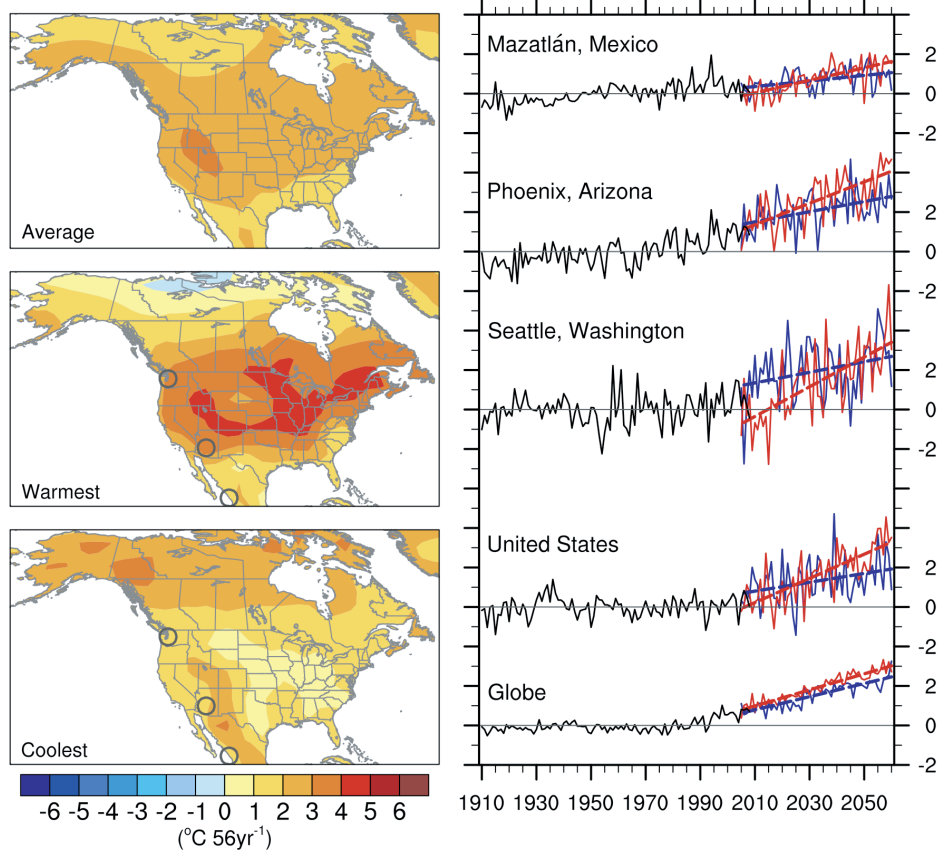


Fig. 5. As in Fig. 4 but for Ensemble Members #3 and #31, the most contrasting runs in JJA. From Deser et al., (2012b).

semble-mean projection. It follows that unless the CCSM is seriously underestimating the role of soil moisture feedbacks, regional precipitation trends forced by the buildup of greenhouse gases are not likely to become detectable above the internally generated background variability in the observations until well beyond 2060.

2.2. Observed and simulated 20th Century trends

Historical reconstructions of the climate of the 20th century provide an even more graphic illustration of the inherent difficulties in comparing an individual realization (in this case, the historical record) with an ensemble of nu-

merical simulations. Figure 7 shows 1970–2005 wintertime surface air temperature trends for individual ensemble members of suites of historical simulations conducted with the CCSM4 and ECHAM5 models. These initial-condition historical ensembles follow a similar experimental design as the 21st Century ensembles discussed above (Deser et al. 2013). CCSM4, introduced in 2010, is more advanced than CCSM3 in several important respects (Gent et al. 2011). The patterns for the historical reconstructions are even more diverse than the ones shown in Figs. 4-6 because the interval over which the trend is computed is 36, rather than 56 years, and is thus subject to smaller anthropogenic forcing and larger sampling variability.

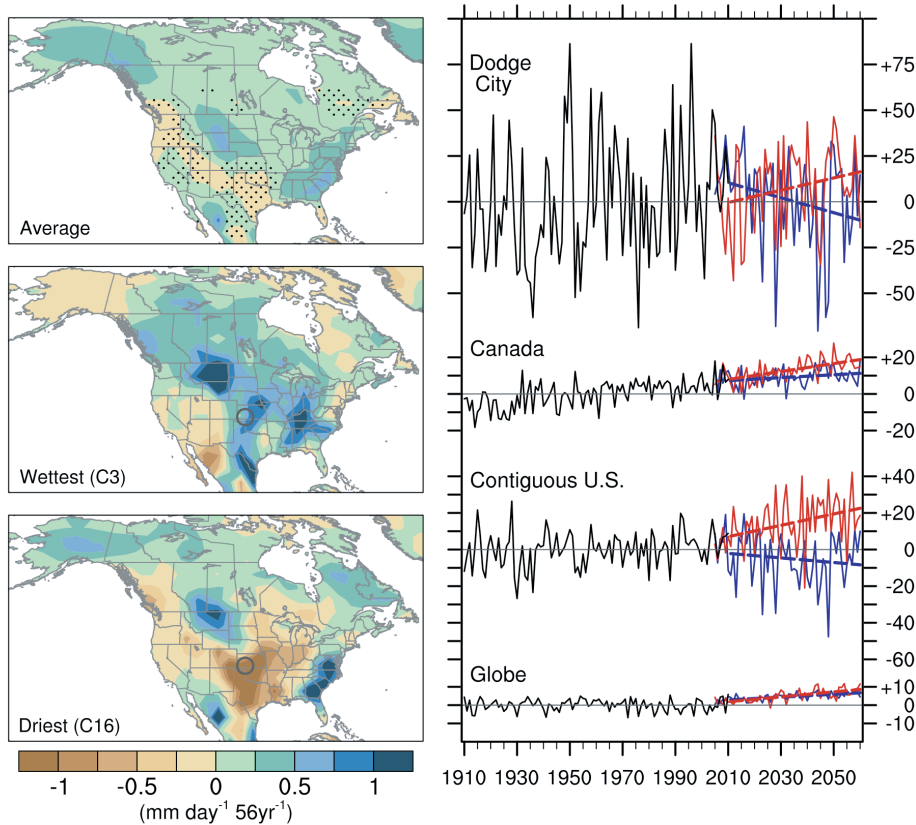


FIG. 6. As in Fig. 4 but for summer (JJA) precipitation.

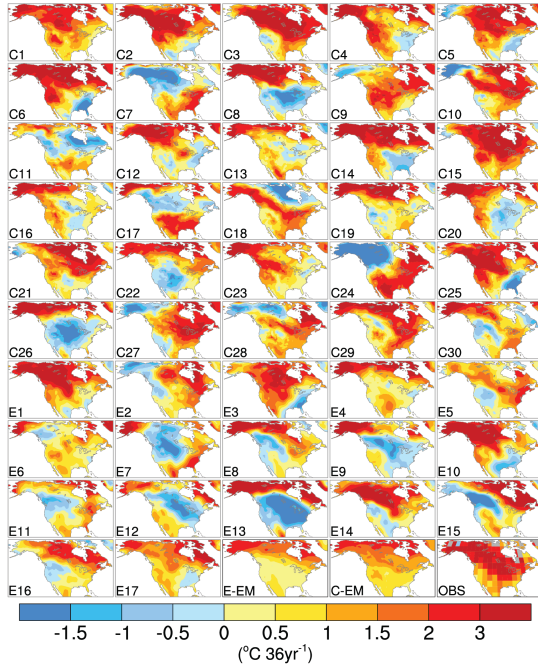


FIG. 7. DJF surface air temperature trends for the reference interval 1970–2005 in a 30-member ensemble of the CCSM4 (C1–C30) and 17-member ensemble performed with the ECHAM model (E1–E17). Trends are expressed in $^{\circ}\text{C}$ per 36 years. The ensemble-mean trend and the observed trend for this period are shown at the end of the sequence of maps.

In the context of these simulations, the observational record is just one of the many possible outcomes of the time dependent forcing that the climate system has been subject to over the past century. Let us now consider the observed trends in greater detail. Figure 8 shows time series of observed and simulated trends in (a) global mean surface temperature including both land and ocean, (b) global-mean surface air temperature over land and (c) cold season surface air temperature poleward of 40°N . The simulations in this case are based on the reference interval 1965–2000 (5 years earlier than the one used in the simulations described in Fig. 7, but 30 out of the 36 years of the two records are overlapping. Both intervals 1965–2000 and 1970–2005 were marked

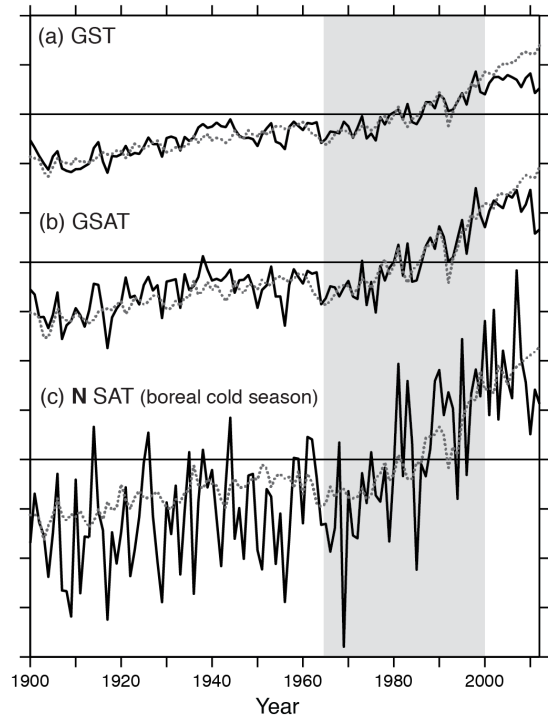


Fig. 8. Observed (*solid*) and multi-model ensemble mean (MEM) (*dotted*) temperature anomaly time series with respect to the 1965–2000 reference period (indicated by light gray shading) for (a) annual-mean, global-mean surface temperature (GST), (b) annual-mean, global mean land temperature (GSAT), and (c) boreal cold season-mean (Nov.–Apr.) land temperature poleward of 40°N . Tick marks on the abscissa denote intervals of 0.5°C . Observations from NOAA merged ocean land surface temperature dataset. Model output based on AR4 (CMIP3) historical simulations in which ozone depletion and volcanic aerosols are included as part of the forcing (1900–1999) and SRES A1B simulations (2000–2012). Adapted from Wallace et al. (2012).

by pronounced warming that was more rapid over land than over the oceans, as shown in Fig. 8a,b and the high latitude Northern Hemisphere continents warmed about three times as much as annual mean GST during the boreal cold season (Fig. 8c).

The GST time series based on the multi-member ensemble mean of the CMIP simulations closely tracks the observations during the reference period 1965–2000 but it fails to cap-

ture the flattening of the curve in the past decade. As of the end of 2012 the projections were $\sim 0.4^\circ\text{C}$ higher than the observed GST.

Figure 9 shows the spatial distribution of the observed 1965–2000 SAT trends during the boreal cold and warm seasons (a,c) together with multi-model ensemble means of numerical simulations that were used as a basis for the Fourth Assessment Report of the IPCC (b,d; Randall et al. 2007; Meehl et al. 2007): the simulations include nine different models with ensemble sizes ranging from 1 to 5. Consistent with the modeling results presented in the previous subsection, the multi-model ensemble-mean trends are much more spatially homogeneous than the observed trends, particularly over high northern latitudes during the boreal cold season. The observed warming trends over Siberia and Canada during this interval, which ranged up to $\sim 3^\circ\text{C}$ per 36 years, were an order of magnitude larger than the mean rate of global (GST) warming during the 20th Century ($\sim 0.08^\circ\text{C}$ per decade). They

are also larger and extend farther southward than the corresponding multi-model ensemble mean trends shown in the right hand column of Fig. 9. Hence, it seems quite likely that the enhancement of the warming was either thermodynamically- or dynamically-induced by the free (internally generated) variability of the climate system; *i.e.*, the categories listed in the bottom row of Fig. 1.

Over the 92-year-long reference interval 1920–2011 the regional SAT trends shown in Fig. 10, expressed in $^\circ\text{C}$ per 92 years, are smaller than those for the shorter reference interval shown in the previous figure, but they still range up to nearly 3°C per century, about three times the GST trend. The heterogeneity of the trends during the boreal winter shown in Fig. 10a, and the fact that they are so much larger than the corresponding warm season trends shown in Fig. 10b suggest that even on this extended time scale, the internal variability of the climate system makes an important contribution to the observed trends.

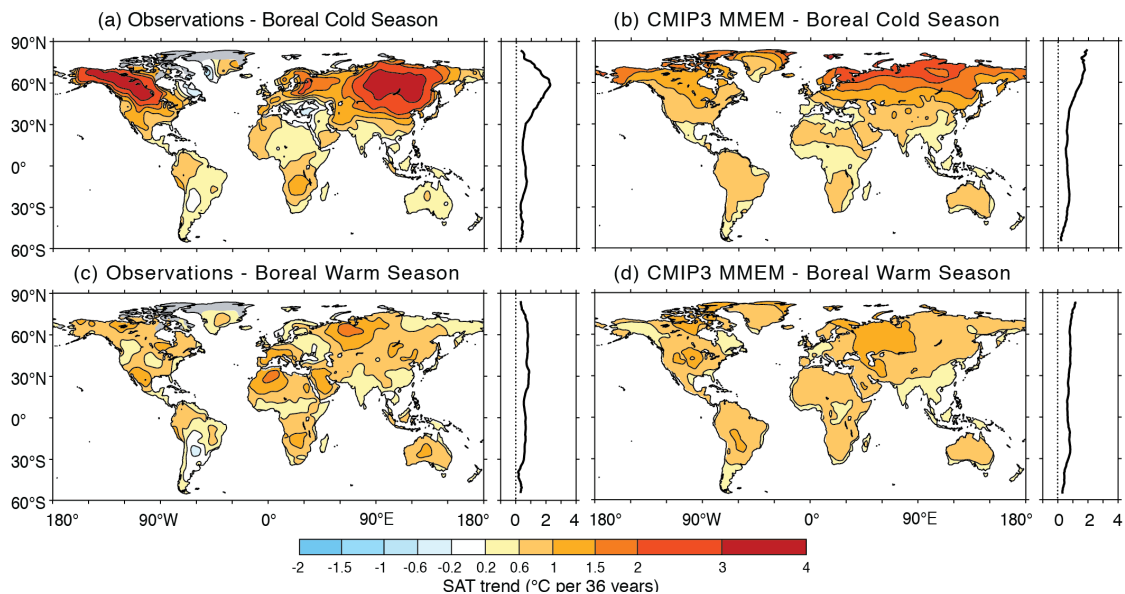


Fig. 9. Maps and zonally averaged meridional profiles showing rates of warming (*i.e.*, the linear trend) over the historical reference interval 1965–2000 expressed in units of $^\circ\text{C}$ per 36 years: (a,b) boreal cold season; (c,d) boreal warm season. Left column (a,c) based on observations and right column (b,d) the multi-model ensemble mean (MMEM) of the AR4 simulations. From Wallace et al. (2012).

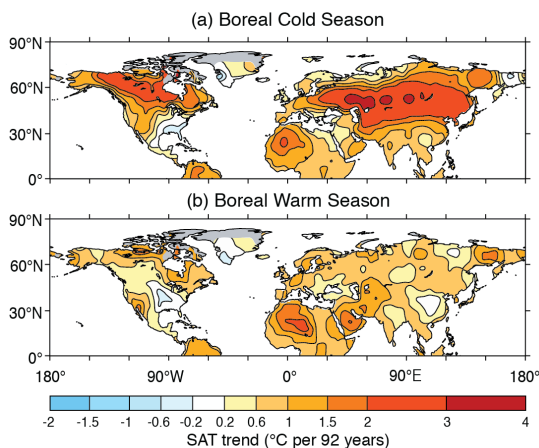


FIG. 10. Observed rates of warming in SAT over the historical reference interval 1920–2011 (*i.e.*, the linear trend) expressed in units of $^{\circ}\text{C}$ per 92 years: (a) boreal cold season; (b) boreal warm season. Based on the NCDC MLOST dataset.

3. Assessing the dynamically-induced variability

As noted in the Introduction, dynamically-induced variability of SAT and rainfall (*i.e.*, variability attributable to the time-varying atmospheric circulation) is not identical to the internally generated variability for two reasons: (1) anthropogenic forcing can induce changes in the atmospheric general circulation and (2) internal variability of the climate system would be capable of inducing changes in SAT, even in the absence of circulation changes. These distinctions are reflected in the categories of causal mechanisms in Fig. 1. But despite these caveats, it appears that much of the internally generated variability in the SAT field is mediated by changes in the atmospheric circulation. To illustrate this point, we reexamine Ensemble Members #4 and #22 from the CCSM3 40-member ensemble, whose SAT fields were depicted in Figs. 4, 5, and 6, but here in Fig. 11a,b we show them together superimposed on the corresponding trends in

the sea level pressure (SLP) field. The SLP trend in Member #4 is in the sense as to favor offshore flow along the west coast from British Columbia to California, reducing the moderating influence of the influx of marine air masses upon winter temperatures over most of North America. In contrast, the trend in Member #22 (Fig. 11b) is in the sense as to increase the onshore flow over western Canada. That the strength of the onshore flow along the Pacific seaboard exerts a strong influence on wintertime SAT over the continental US is borne out in the Member #22 minus Member #4 SLP difference map shown in Fig. 11c, and the regression map based on all the other ensemble members shown in Fig. 11d. It is notable that the SLP trends in these “outlier” members of the 40-member ensemble are much larger than the ensemble-mean SLP trend shown in Fig. 2a. The same must be true of randomly selected members because at most grid points the ensemble-mean 56-year trend is less than 0.5 standard deviation of the trends in the individual ensemble members, as shown in Fig. 2b. In agreement with this conclusion, based on an analysis of simulations performed with CMIP3 models, Oshima et al. (2012) reported that the contribution of internal climate variability the diversity of century-long SLP trends over the North Pacific in the ensemble members is as large as the ensemble mean trend itself and that internal variability accounts for virtually all of the diversity of the 50-year SLP trends in the individual ensemble members during the first half of the 20th century.

Is it merely chance coincidence that the SLP trends in Ensemble Members #4 and #22 are dynamically consistent with the contrasting SAT trends over the continental United States? To address this question we show in

Fig. 11d the pattern of DJF SLP trends regressed on the standardized SAT trends averaged over the continental United States in the other individual ensemble members. That the

SLP patterns in Figs. 11c,d are broadly similar confirms the inference that the differences in the SAT trends in the individual ensemble members are at least to some degree dynami-

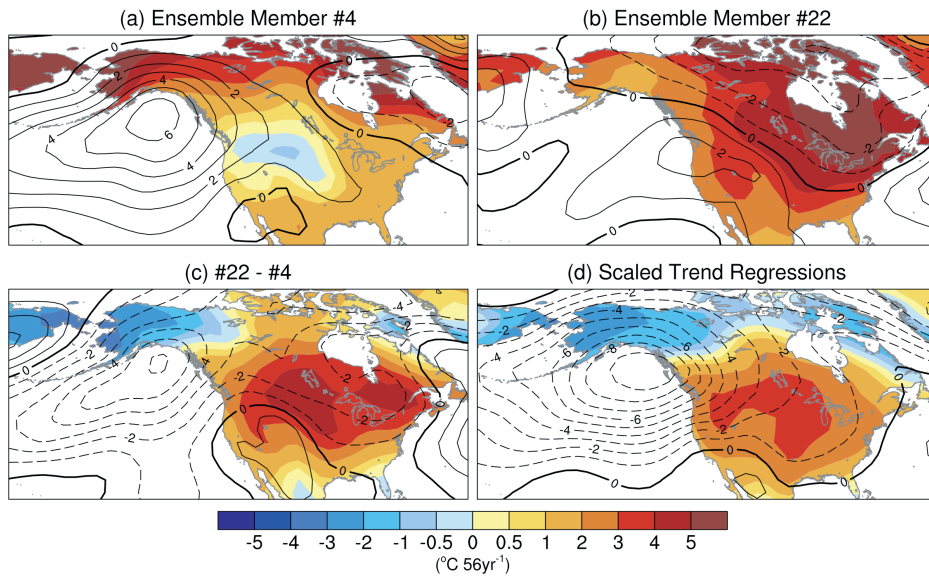


FIG. 11 (a,b) 2005-2060 DJF SAT trends in Ensemble Members 4 and 22 of the CCSM3 40-member ensemble, (c) The difference between (a) and (b). (d) Trends in the individual ensemble members (exclusive of #4 and #22) regressed on the 38 corresponding raw SAT trends averaged over the continental US. SAT trends are indicated by colored shading and SLP trends by contours. Contour interval 1 hPa per 56 years. The zero contour is bold and dashed contours indicate SLP falls.

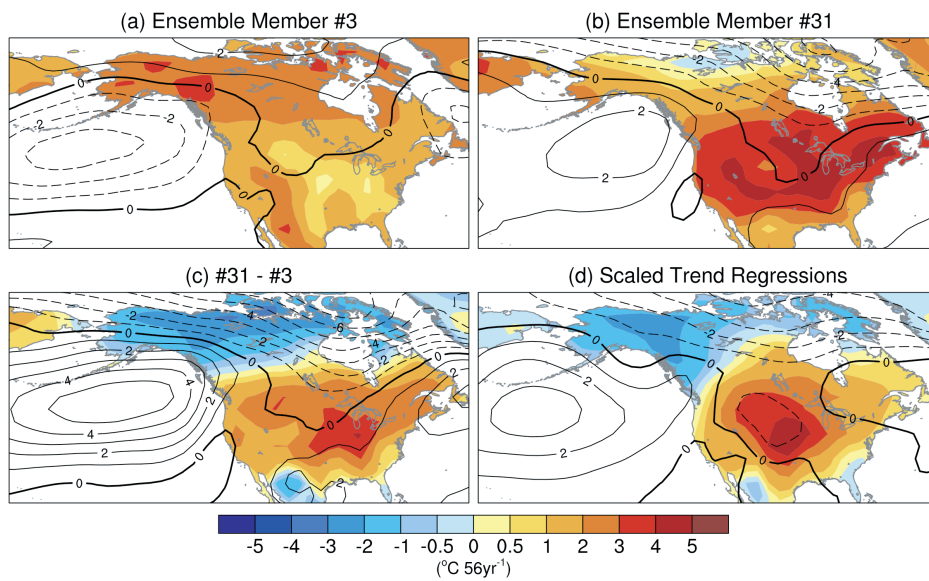


FIG. 12. As in Fig. 11 but for SAT and SLP in JJA, contrasting the two ensemble members that exhibit the weakest (#3) and strongest (#31) SAT trends averaged over the contiguous US.

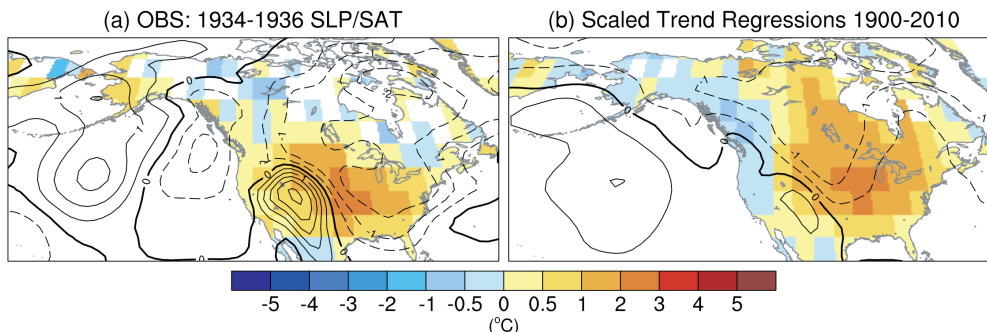


FIG. 13. (a) Pattern of SLP anomalies (contoured) and SAT anomalies (shaded) during the US Great Plains Dust Bowl summers, the average of JJA 1934, 1935, and 1936. The reference period for the anomalies is 1900-2010. (b) SLP and SAT regressed on the detrended time series of JJA SAT averaged over the continental US. The regression coefficients are based on the period of record 1900-2010, exclusive of JJA 1934, 1935, and 1936. Contour interval 0.5 hPa. Based on the 20th Century Reanalyses (Compo et al. 2011).

cally induced.

Analogous results for ensemble members with contrasting summertime 2005–2060 SAT trends are shown in Fig. 12. These runs exhibit contrasting patterns of SLP trends over the North Pacific and over the Canadian Arctic, but distinctions between the warm and cold patterns are not as clearly discernible over the contiguous US. That the JJA SLP trends in the other 38 ensemble members regressed upon the respective SAT trends averaged over the continental United States yields (Fig. 12d) yields a pattern similar to the difference map (Fig. 12c) is suggestive of a dynamical influence upon the SAT trends in the individual ensemble members in summer as well as in winter.

Patterns of SLP and SAT anomalies observed during anomalously hot summers over the contiguous US the so-called “Dust Bowl” and, more generally during hot summers over CONUS are shown in Fig. 13. The anomalous upstream anticyclone over the North Pacific and the anomalously low SLP along the Arctic coast are not as prominent in the historical data as they are in the simulated SLP patterns shown in the previous figure. Apart from the

anomalies over the regions of elevated terrain over the southwestern US, which is mainly a SAT signature, the SLP anomalies are quite small. It is difficult to understand how the low level circulation anomalies associated with such weak features could have been responsible for the large SAT anomalies either in the simulations (Fig. 12) or in extreme years in the historical record (Fig. 13). Feedbacks involving soil moisture could greatly increase the amplitude of the internal variability of SAT, at least in the model. The land surface tends to become drier as it warms and, conversely, summer SAT tends to be warmer over dry land surfaces. Both relationships contribute to a negative correlation between temperature and precipitation. In the CCSM3 ensemble members with strong summertime warming trends over the continental US tend to be marked by negative precipitation trends and vice versa: the correlation coefficient between JJA SAT trends and precipitation trends averaged over the continental US among the 40 individual ensemble members is -0.82 . Dry months also tend to be warmer than normal in the observations (Madden and Williams 1978; Trenberth and Shea 2005) but the negative

correlation between precipitation and SAT is not as strong. A drying tendency favors a tendency toward reduced latent heat fluxes and enhanced sensible heat fluxes at the Earth's surface, which favors warming. Such land surface feedbacks can serve to amplify and prolong dynamically-induced heat waves (e.g., see Black et al. 2004 or Dole et al. 2012), rendering internally generated dynamically- and thermodynamically-induced diversity in the temperature trends difficult to separate, even in large ensembles of simulations.

3.1. Further insights derived from projections of future SAT trends

The 40-member ensemble of CCSM3 simulations in Deser et al. (2012a) has been subjected to a more formal analysis of the dynam-

ical contribution to the diversity of the winter-time SAT trends. The left hand columns of Fig. 14 show the leading Northern and Southern Hemisphere empirical orthogonal functions (EOFs) derived from the extratropical DJF and JJA 2005-2060 SLP trends. In the climate literature EOF analysis is usually performed in the space / time domain and the “modes” obtained from it consist of an ordered set of spatial patterns (EOFs) whose time-varying amplitudes and polarities are described by their respective principal component (PC) time series. In Deser et al. (2012a) the analysis is performed in the domain of space / ensemble number: the EOFs are spatial patterns but in their analysis the PCs refer to the amplitude and polarity of various 2005-2060 trend EOFs as expressed in the individual ensemble members. Despite the differences

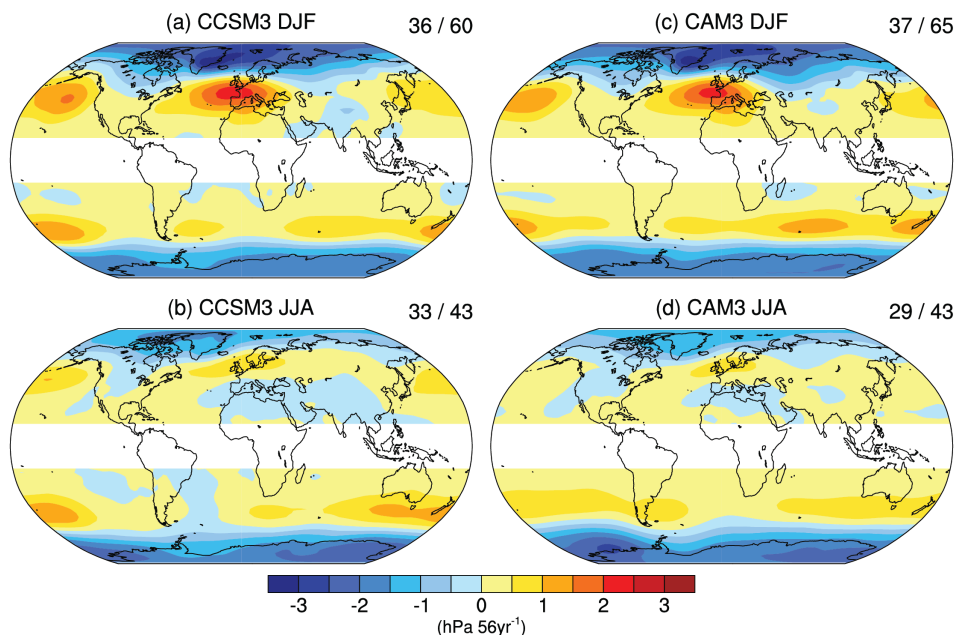


FIG. 14 The leading EOFs of extratropical SLP trends from the 40-member CCSM3 ensemble (a) DJF and (c) JJA; and in the CAM3 ensemble (b) DJF and (d) JJA. Trends are computed over the period 2005–2060 for CCSM3 and for 56-year non-overlapping segments for CAM3. EOF analysis is performed for each hemisphere separately but plotted on a single map. The percent variance explained by each EOF is given in the upper right corner of each panel, with the first number denoting the NH and the second number the SH (for example, for CCSM3 in DJF, NH EOF1 accounts for 36% of the NH variance and SH EOF1 accounts for 60% of the SH variance). From Deser et al. (2012a).

in which that data are analyzed, the DJF SLP patterns and the Northern Hemisphere JJA pattern shown in Fig. 14 closely resemble the leading EOFs of the month-to-month variability in historical time series (Thompson and Wallace 2000; not shown), which are commonly referred to as the “Northern and Southern Hemisphere annular modes” (NAM and SAM, respectively; we will refer to them by those names). They correspond to preferred modes of variability in the historical record and in extended control runs of the CCSM3 and other climate models (Miller et al. 2006).

The CCSM is a coupled model in which ENSO and longer term climate variations resulting from large-scale atmosphere-ocean

interactions come into play. In order to distinguish between the internally generated variability that is attributable to changes in the atmospheric circulation alone and variability that is a consequence of atmosphere-ocean interactions, the SAT trends in the 40-member ensemble of CCSM3 runs are compared with trends in non-overlapping 56 year segments of a 10,000 year control integration of the Community Atmospheric Model (CAM3), the same atmospheric model that is used in the coupled CCSM3 integrations. In the control integration greenhouse gas and aerosol concentrations are held constant and SST is prescribed in accordance with the seasonally varying climatology but the treatment of land sur-

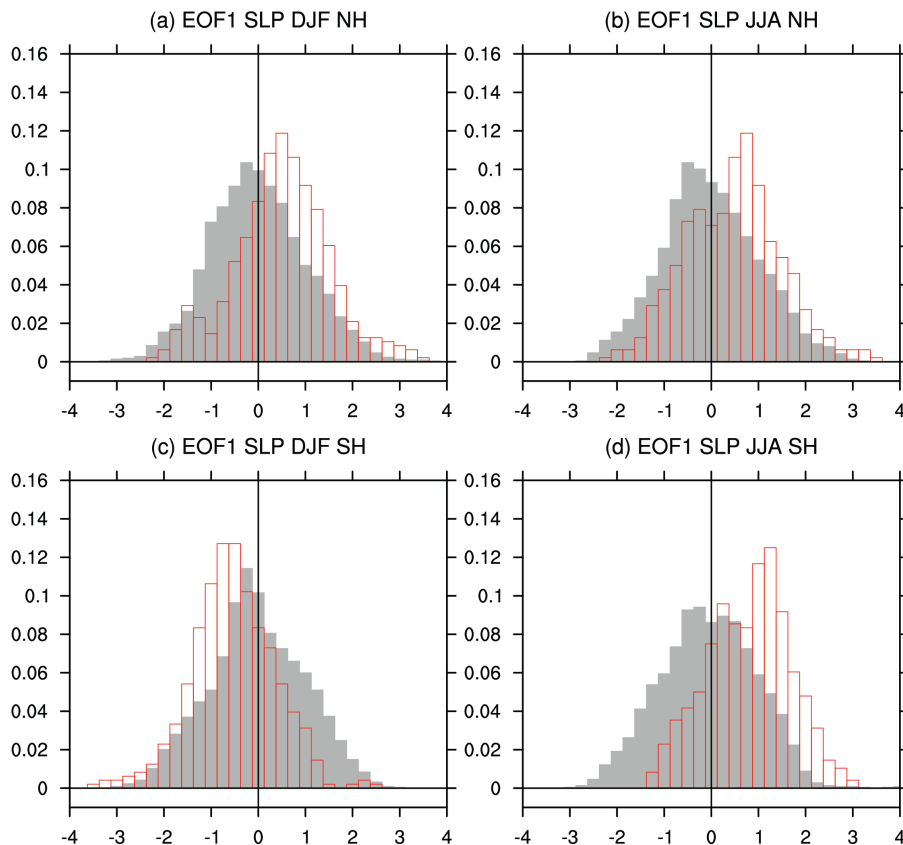


FIG. 15. Histograms of the SLP 2005–2060 trend projections onto EOF1 from the CAM3 control integration broken down by hemisphere and season as indicated. The red open bars show results from the 40-member CCSM3 and the gray filled bars from the 178-member Community Atmospheric Model (CAM3), which is used as a control. The x axis is in units of standard deviations of the CAM3 control integration, and the y axis is frequency (number of ensemble members divided by the total number of ensemble members). From Deser et al. (2012a).

face feedbacks is the same as in CCSM3. Results are shown in the right hand panels of Fig. 14. If the atmosphere-ocean coupled variability were making an important contribution to the diversity of the trends among the CCSM3 ensemble members, one would expect the amplitude of the annular modes and other preferred patterns of variability in the SLP field to be larger in the CCSM3 ensemble members than in the 56-year segments of the CAM simulations. That the EOFs obtained from the CCSM3 and CAM3 runs are similar in shape, comparable in amplitude, and explain comparable fractions of the total SLP variance suggests that the diversity of the SLP trends in the CCSM3 ensemble members is mainly due to the internal variability of the atmospheric circulation in the absence of any coupling to the ocean.

The ensemble mean of the trends in the 56-year segments of the CAM3 control run is indistinguishable from zero. However, the projections of the patterns of SLP trends in the 40 CCSM3 simulations onto EOF1 of the control run shown in Fig. 15 exhibit a statistically significant positive bias indicative of falling SLP in both polar cap regions and rising SLP over much of middle latitudes. SLP changes in this sense are commonly referred to as a trend toward the “high index polarity” of the NAM and the SAM. Nearly all the climate models used in the IPCC projections exhibit a trend in this sense (Meehl et al. 2007). This shift toward the high index polarity of the annular modes is evidently a robust feature of the ensemble-mean response to the buildup of greenhouse gases in the CCSM3 (*i.e.*, the upper right box in Fig. 1), but it is expressed with different strengths in different ensemble members and in some members the trend is in the opposite sense. The diversity of the SLP

trends in the individual members of the ensemble, as reflected in the width of the frequency distributions in Fig. 15, is a measure of a kind of structural uncertainty inherent in the projected SLP trends for 2005–2060.

The low level circulation pattern implied by EOF1 of the SLP trend induces a spatially varying SAT trend of the form shown in Fig. 16, which is obtained by averaging the SAT trends over all ensemble members, weighting each in accordance with the projection of its pattern of SLP trend upon EOF1 (*i.e.*, by its value of PC1). The patterns of induced SAT trend in the two hemispheres are dynamically consistent with EOF1 of the SLP trend and they resemble the SAT patterns obtained by regressing the SAT field upon time varying (SLP) indices of the annular modes (Thompson and Wallace 2000). The regression patterns in Fig. 16, in effect, define the anomaly in the trend of SAT in each member of the ensemble (*i.e.*, the departure from the ensemble-mean SAT trend) that can be attributed to

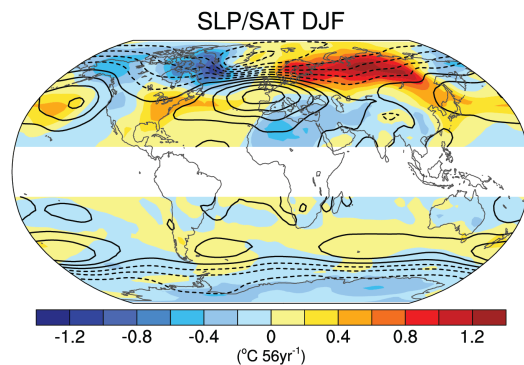


FIG. 16. Surface temperature regressed upon the scores of EOF1 of extratropical SLP trends from the 40-member CCSM3 ensemble in DJF, shown in Fig. 15. Contours show the SLP trend EOF (contour interval 0.6 hPa per 56 years; negative values are dashed). Trends are computed over the period 2005–2060. EOF and regression analyses are performed for each hemisphere separately but plotted on a single map. From Deser et al. (2012a).

the anomalous trend in the NAM/SAM in each ensemble member (again, anomalous with reference to the ensemble mean trend). Subtracting out that portion of the SAT trend at each grid point in each ensemble member that is attributable to the anomalous trend in the NAM/SAM in that ensemble member constitutes a *dynamical adjustment* that serves to reduce the diversity of the trends among the ensemble members. A *dynamically adjusted* global or hemispheric SAT trend field can be created by subtracting the dynamical contribution from the raw SAT trend field for each member. In principle, a complete dynamical adjustment of the SAT trends in the individual members of the ensemble can be obtained by the applying dynamical adjustments not only for the NAM/SAM, but for all the significant EOFs of the SLP trends. In practice, applying this procedure to an ensemble with a finite number of members will inevitably tend to overestimate the dynamical contribution. The challenge is to limit the degree of “overfitting.”

3.2. *Estimating the dynamical adjustment for individual ensemble members*

In order to avoid serious overfitting of the diversity (or variance) of the trends in the individual ensemble members it is necessary to apply analysis techniques that are parsimonious i.e., that involve regression equations containing very few SLP predictors. Deciding how best to perform the analysis is an area of active research. Here we will briefly describe some of the linear analysis tools that might be used in performing such an analysis.

Consider the set of SAT trends $T(n)$, ($n = 1, N$) at a specified grid point, one belonging to each of the N ensemble members. A simple, conservative approach is to apply least

squares regression (LSR), using the SLP trend field in a prescribed spatial domain to define a single “predictor” $T^*(n)$ of $T(n)$. The first step is to regress the standardized SLP trend field upon $T(n)$ to obtain a single predictor pattern $P(x)$. Here the standardization is performed in “ensemble-space”; i.e., the standard deviation of SLP trend at each grid point is based on the sample consisting of the N ensemble members. The second step is to project the standardized SLP trend field in each ensemble member upon $P(x)$ to obtain a “score” $S(n)$ that provides a relative measure of the polarity and the strength with which the predictor pattern $P(x)$ is expressed in that ensemble member. The final step is to scale the scores $S(n)$ by fitting them to $T(n)$ using the method of least squares. The rescaled scores are the predictors $T^*(n)$, which constitute the dynamical adjustment. Spatial averaging and the steps in LSR are commutative, so this procedure can equally well be applied directly to an ensemble of spatially averaged SAT trends such as $GST(n)$.

For each specified grid point or area average time series, LSR yields a single correlation coefficient or “predictor” $T^*(n)$ of the SAT trend in the n th ensemble member and is thus as parsimonious as any method can be. The LSR approach can be extended to multiple predictors by the method of partial least squares regression (PLSR). In PLSR, the first predictor $T_1^*(n)$ is obtained by LSR, as described above. A residual data set is then created by regressing $T_1^*(n)$ out of both the SLP trend field in each of the individual ensemble members (i.e., the field from which the “predictor patterns” are chosen) and the ensemble of grid point or area-average SAT trends $T(n)$ (the “predictand”). Then LSR is applied to these residuals to obtain a second predictor $T_2^*(n)$ that is orthogonal to $T_1^*(n)$ by con-

struction and a second set of residuals. The procedure can be repeated as many times as desired. PLSR is widely used in other fields such as econometrics, chemometrics, neuroscience, and computer science, and is beginning to be more widely used in geophysics (Smoliak et al. 2010). It has been used by Wallace et al. (2012) to estimate the dynamical contribution to the wintertime SAT trends over the Northern Hemisphere continents, as discussed in the next subsection.

The above procedure can be computationally intensive when it is applied *pointwise* (i.e., to every grid point in the SAT field) because of the high degree of redundancy inherent in the calculations, especially when the grid is fine. Under some circumstances it may

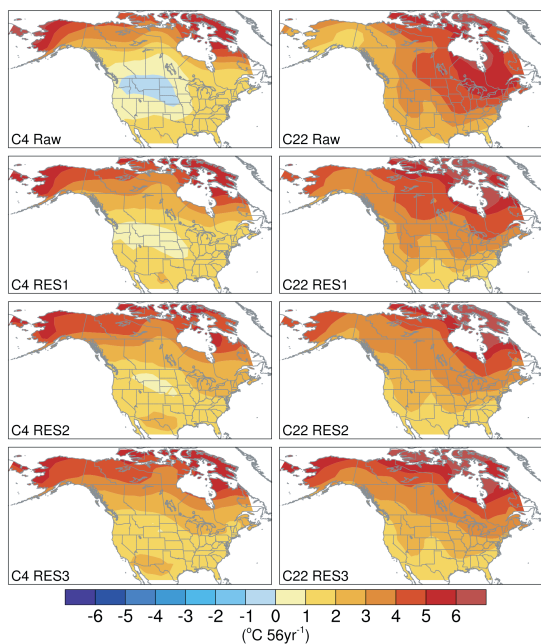


FIG. 17. Examples of raw and dynamically adjusted 2005-2060 SAT trends for ensemble members 4 (*left*) and 22 (*right*) of the 40-member CCSM3 ensemble, the members that exhibited the smallest and largest SAT trends averaged over the contiguous US. The top row of panels show the raw patterns, the second shows the adjusted patterns with one pass of PLSR, the third row with two passes, and the bottom row after three passes.

be preferable to expand the SAT trend field in terms of EOFs and to perform LSR or PLSR on a subset of the resulting PC time series. The same considerations that apply to pointwise or area-wise LSR/PLSR are also applicable when these forms of analysis are performed in PC space.

Figure 17 shows raw and dynamically adjusted wintertime SAT trends for Members #4 and #22 of the 40-member ensemble conducted with CCSM3, the ensemble members with the smallest and largest SAT trends over CONUS. In this example the dynamical adjustment was computed by performing pointwise PLSR on the SAT field over North America. The patterns $P(x)$ in the SLP field are for the domain 10° to 90°N and from the Date Line to the Greenwich Meridian. The dynamical adjustment has the strongest influence on outlier ensemble members such as these. With each

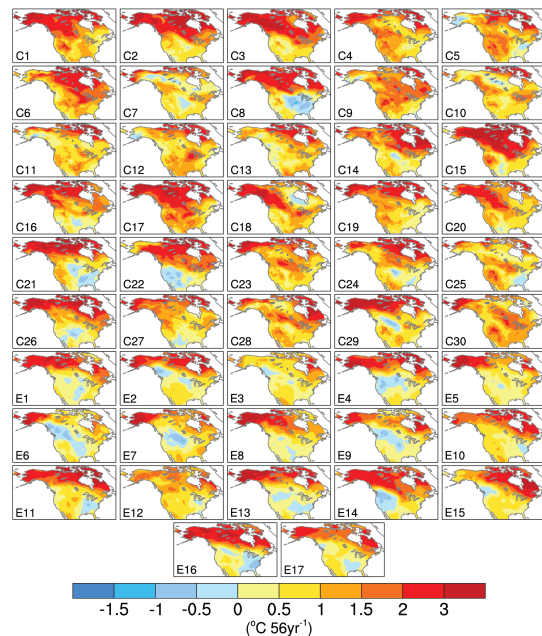


FIG. 18. As in Fig. 7 but dynamically adjusted with two passes of PLSR using the SLP field in the domain 10° to 90°N and from the Date Line to the Greenwich Meridian as the predictor field.

pass the contrast between the two ensemble members becomes less pronounced.

Figure 18 shows dynamically adjusted trends for the individual members of the CCSM4 and ECHAM ensembles, whose raw trends were shown in Fig. 7. Application of the dynamical adjustment substantially reduces the diversity of the SAT trend patterns in the ensemble members, bringing them more into line with the ensemble-mean trends. Averaged over the North American domain, applying this dynamical adjustment with two passes accounts for 75% of the variance of the SST trends in the 30-member CCSM4 ensemble. That it leaves 25% of the variance unexplained suggests that our dynamical adjustment scheme, which relies exclusively on the SLP field, might not be capturing all the dynamically-induced variance.

When applied to regions the size of the CONUS, the dynamical adjustment based on SLP appears to be even more effective in reducing the diversity of the SAT trends in summer than in winter, accounting for 81% of the variance of the SST trends in the 30-member CCSM4 ensemble with only two passes.

3.3. Dynamically adjusting SAT trends in the historical record

To adapt the methods described in the previous subsection to estimating the dynamical contribution to the observed SAT trends it is necessary to use temporal variability within the historical record as a surrogate for the diversity of the individual ensemble members in the simulations. In this case the goal is to explain the multidecadal variability of the trends observed within a single time series using SLP patterns derived from the analysis of that same time series. The strong late 20th Century

warming trend during the boreal cold season over the continental interiors documented in Section 2.2 is arguably the most dramatic feature in the historical record. Was it dynamically induced? If so, is the adjustment large enough to affect estimates of the rise in annual mean GST during this period?

As background for addressing this question, Fig. 19 shows the global pattern of November-April SLP trends from 1965 to 2000. Compared to other sampling intervals of comparable length, the trends during this interval are particularly strong and spatially coherent, with pressure falls in both polar regions and pressure rises in midlatitudes, indicative of a shift toward the high index polarity of the NAM and the SAM. The trend in the PNA pattern was associated with a spontaneous, abrupt shift toward a more El Niño-like state of the sea surface temperature distribution and related atmospheric circulation patterns equatorial Pacific in 1976-77 (Nitta and Yamada 1989; Trenberth and Hurrell 1994; Zhang et al. 1997).

Shindell et al. (2001) investigated the cause of the strong NAM-related trends during this interval and they concluded, on the basis of numerical simulations with an array of external forcings, that the observed trend in the NAM during this interval was beyond the range of internal variability and was likely forced by a change in the meridional heating gradient in the stratosphere induced by the buildup of greenhouse gases. This explanation would account for the prominence of the NAM signature in the 1965-2000 SLP trend but does not explain the reversal in the trend in the NAM that began in the mid- 1990s and became more clearly apparent after the turn of the millennium (see NCAR's Climate Data Guide, <http://climatedataguide.ucar.edu>, for a

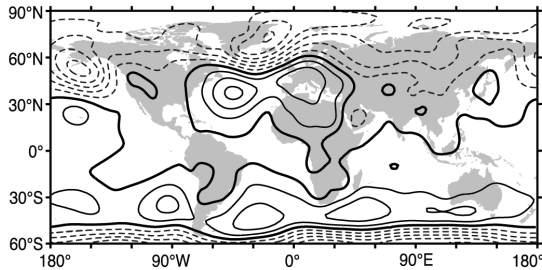


FIG. 19. Observed 1965–2000 SLP trends for the boreal cold season (Nov.–Apr.), based on the 20th Century Reanalyses. The contour interval is 1 hPa per 36 years. Negative values are dashed. Zero contour bold. From Wallace et al. (2012).

NAM index from 1899 to present). Subsequent numerical experiments by Bracco et al. (2004) and Deser and Phillips (2009) based on ensembles of integrations with two atmospheric GCMs forced with the observed evolution of SSTs, greenhouse gases, ozone and aerosols suggest that the prominent NAM signature in Fig. 19 is likely a manifestation of atmospheric internal variability that happened to be particularly strong during this 36-year interval.

In a similar manner, Trenberth and Hoar (1996, 1997) investigated the cause of the late 20th Century trend toward the positive polarity of the PNA pattern; i.e., the prevalence of an El Niño-like state of the tropical Pacific after the mid-1970s. On the basis of a statistical analysis of the historical record of the Southern Oscillation Index (SOI) they concluded in their second paper that the behavior of the SOI during the post 1976 period had been “highly unusual and very unlikely to have been caused by natural variability”. With the benefit of 15-years of hindsight it is evident that the role of natural (*i.e.*, unforced) variability of the climate system was underestimated in this case as well: the prevalence of the El Niño-like state of the equatorial Pacific

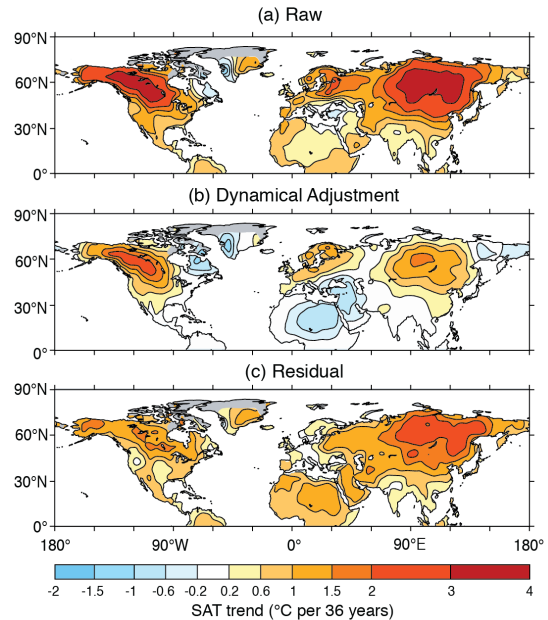


Fig. 20. 1965–2000 SAT trends for the boreal cold season (Nov.–Apr.): (a) the raw trend pattern, (b) the dynamical contribution, estimated by partial least squares regression (PLSR) with two predictors for each grid point, and (c) the dynamically adjusted trend pattern, calculated by subtracting the dynamical contribution in (b) from the raw trend pattern in (a).

has not persisted into the 21st Century (Hu et al. 2013).

In contrast to the trends in the NAM and the PNA pattern, the late 20th Century trend in the SAM is widely regarded as having been at least partially forced by a decrease in concentrations of stratospheric ozone due to the buildup of CFCs during this period—the so-called “Antarctic ozone hole” (Thompson and Solomon 2002; Gillett and Thompson 2003; Polvani et al. 2011). It has been suggested that the more subtle ozone losses that occurred over the Arctic during this period might have induced an analogous trend in forcing the NAM, but the case is less clear (Hartmann et al., 2000).

The NAM- and PNA/ENSO-related SLP trends have obviously contributed to the win-

tertime warming of Eurasia and North America poleward of 40°N from 1965 to 2000. Results obtained by dynamically adjusting the time series of SAT averaged over all the Northern Hemisphere land grid points poleward of 40°N, using two PLSR Northern Hemisphere SLP predictors, are shown in Fig. 20. The dynamical contribution to the SAT trend resembles the SAT signature of the NAM. The residual SAT trend is weaker than the raw trend and more closely resembles the corresponding warm season trend shown in Fig. 9c. Yet it is clear that the dynamical adjustment shown in Fig. 20 does not account for all of the enhanced warming over the interiors of the continents during the boreal cold season relative to the model simulations shown in Fig. 9b. Either the methodology described in the previous subsection is failing to capture all the dynamically-induced variability or there is a contribution from the thermodynamically-induced internal variability discussed in the next subsection and in Chapter XX.

To place the dynamical adjustment for 1965–2000 in a global context, Table 1 shows a summary of how it affects the trends in global mean SAT over land (GSAT) and over the entire globe (GST). Applying the dynamical

adjustment reduces the warming over the high latitude Northern Hemisphere land masses during the boreal cold season from 1.72°C to 1.02°C over this 36-year interval, eliminating most of the excess warming relative to the warm season and relative to the land lying south of 40°N. The magnitude of the adjustment (0.70°C) is diluted by averaging over all land (to 0.28°C) and over the year (to 0.14°C) and by combining land and ocean data (to 0.04°C in GST). Hence, changing extratropical circulation patterns during the boreal winter accounted for less than 10% of the global warming signal during this interval. Compared to the *accelerated warming*; i.e., the rate of rise of annual mean GST during this interval minus the mean rate of rise of GST during the past century of 0.08°C per decade or 0.29°C per 36 years, it amounts to about 15%. Hence, though appreciable and of first order importance for the attribution of high latitude Northern Hemisphere wintertime temperature trends over land, the dynamical contribution explains only a small fraction of the accelerated global warming during the late 20th Century and even after it is removed, land (GSAT) warmed twice as rapidly as ocean (GSST) during this period.

Table 1. Observed 1965-2000 SAT trends over land for boreal cold and warm seasons November-April and May-October expressed in °C per 36 years. The italicized numbers refer to dynamically adjusted trends as explained in Section 4. GSAT refers to global-mean SAT, GSST to global-mean SST and GST refers to global mean surface temperature including both land and sea. Data based on the National Climatic Data Center historical merged land-ocean land surface temperature analysis (MLOST), with its land component, GHCNv3, and ocean component, ERSSTv3b. Adapted from Wallace et al. (2012).

	Cold	Warm	Annual Mean
N: 40°N–90°N	1.72 (<i>1.02</i>)	0.79	1.26 (<i>0.91</i>)
S: 60°S–40°N	0.70	0.69	0.70
GSAT (Land)	1.03 (<i>0.80</i>)	0.72	0.88 (<i>0.76</i>)
GSST (Ocean)	0.35	0.37	0.36
GST	0.57 (<i>0.49</i>)	0.48	0.52 (<i>0.49</i>)

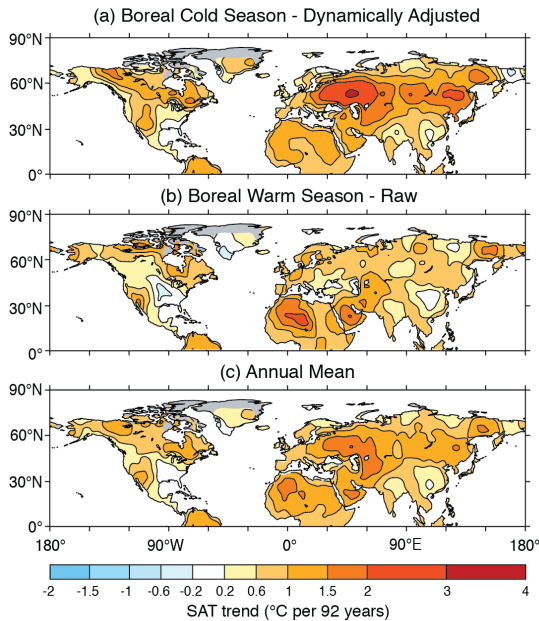


FIG. 21. SAT trend patterns for the reference interval 1920–2011: (a) dynamically adjusted trend for the boreal cold season estimated by PLSR as in Fig. 20, (b) raw trend for the warm season, and (c) annual mean trend estimated by averaging the dynamically adjusted cold season trend and the raw warm season trend.

The importance of the dynamical adjustment tends to decline with the length of the interval over which the trends are computed, but even for the longer interval 1920–2011, it remains quite important during the boreal cold season, as seen in Fig. 21. Applying the dynamical adjustment to the cold season trends and averaging them with the warm season trends is seen to yield a relatively simple spatial pattern suggestive of reduced warming over China and the southeastern United States possibly in response to the buildup of aerosols.

Applying the dynamical adjustment to the cold season trends substantially improves the coherence between cold and warm season SAT time series both for the global mean and for regional means, as illustrated in Fig. 22. In particular, it accounts for most of the excess

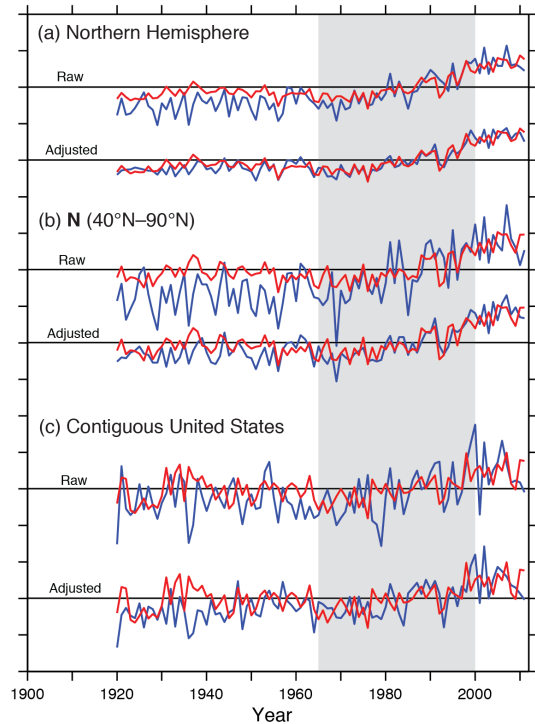


FIG. 22. Time series of (red) warm season and (blue) cold season SAT spatially averaged as indicated. The top pair of curves in each set shows raw time series and the bottom pair shows the dynamically adjusted cold season series and raw warm season series. Adapted from Wallace et al. (2012).

warming during the boreal cold season relative to the warm season over the course of the 20th Century. The positive correlation between the warm and cold season time series on a year-to-year basis is indicative of a season-to-season memory that transcends the very short thermal adjustment time of the land surface. Features such as the cooling following the 1991 eruption of Mt. Pinatubo are more clearly evident in the adjusted data.

4. Does thermodynamically-induced variability play a role?

Of the four categories of processes listed in Fig. 1 that contribute to climate trends, ther-

modynamically-induced internal variability is the most difficult to quantify because it requires an understanding of variations in the oceanic global overturning circulation and the land biosphere and hydrosphere, and in the cryosphere, all of which are on the frontiers of climate science. It is not clear how well the models used in IPCC assessments, including the ones referred to in this chapter, simulate the relevant processes on the multidecadal time scale. For example, it is quite possible that the diversity of the trends in Fig. 7, large though it is, could be underestimated for failure of the models to realistically represent the variability of the ocean circulation for lack of adequate treatment of the physics or proper initialization. In a similar manner, changes in vegetation and ground hydrology that are ignored or not accurately represented in the models could conceivably render the summertime trends more diverse than the examples included in this chapter.

Multidecadal variations in the strength of the meridional overturning circulation in the North Atlantic (MOC) affect the poleward heat transport by the Gulf Stream and its extension to subpolar latitudes and they regulate the rate of exchange of heat between the oceanic mixed layer and the layers below. The temperature of the oceanic mixed layer responds rapidly to changes in the surface energy balance, through which the global warming signal is transmitted together with regional signals associated with atmospheric circulation anomalies. When the MOC is anomalously strong, enhanced poleward heat transports warm the surface waters of the subpolar North Atlantic and parts of the Arctic, which in turn, transfer heat to the atmospheric boundary layer, where it may be advected downstream by the winds. The MOC strength also modulates

the rate at which heat that accumulates in the ocean mixed layer is transferred into the deeper ocean (Meehl et al. 2013). Hence, variations in the strength of the MOC could act as a time-varying thermodynamic forcing of SAT that is likely to be strongest over the higher latitudes during the boreal cold season, when the sea to air fluxes of sensible and latent heat are strongest.

In the absence of reliable direct measurements of variations in the strength the MOC, much of what is known about its role in multidecadal climate variability is inferred from numerical simulations of the oceanic response to prescribed surface forcing as in Alvarez-Garcia et al. (2008). The induced MOC-related variations in the oceanic circulation can feed back on the surface fluxes and thereby force the atmosphere on the interdecadal time scale. Numerical experiments by Semenov et al. (2010) with a coupled model with interactive MOC-related variability suggest that the modulations in the fluxes may have been strong enough to force significant SAT anomalies over the high latitude continents, irrespective of any related circulation changes. If so, the resulting thermodynamic contribution to the high latitude warming would appear in the residual SAT trend field in Fig. 20c.

A prominent feature of the multidecadal variability in the strength of the MOC is the so-called Atlantic Multidecadal Oscillation (AMO), which exhibits a period on the order of 70 years, as discussed in Chapter XX. There and in Chapter XX it is argued that the AMO is a manifestation of internal variability of the coupled atmosphere-ocean climate system that would exist even in the absence of external forcing. It has further been argued that AMO-related variations in the strength of the MOC during the 20th century are respon-

sible for much of the multidecadal variability in the rate of rise of GST; i.e., the relatively rapid rise in the 1920s and 30s, the mid-century hiatus, the resumption of the rapid warming toward the end of the century and perhaps even the recent second hiatus (Del-Sole et al. 2011; Wu et al. 2011; Gulev et al. 2013). For further discussion, the reader is referred to Chapter XX by K. K. Tung).

Another way in which the exchange of water between the mixed layer and the deep ocean on a decadal time scales could exert a thermodynamic influence global surface temperature is through the wind-driven zonal overturning circulation in the equatorial Pacific, which pumps cold water from below the thermocline into the warm ocean mixed layer. The stronger the equatorial trade winds, the stronger the zonal overturning circulation and the sea surface temperature (SST) contrast between the cooler eastern Pacific and the so-called Indo-Pacific warm pool” in the west. Conversely, the stronger the east-west SST contrast, the stronger the trade winds. The existence of this strong positive feedback gives rise to pronounced variability of SST and wind on time scales ranging from seasons to decades. It plays an essential role in the ENSO cycle, but it would exist even in a hypothetical atmosphere coupled to a passive ocean mixed layer (Kitoh et al. 1999; Dommenges 2010; Clement et al. 2011). Based on experiments with numerical models, Meehl et al. (2011) and Kosaka and Xie (2013) have shown evidence that an intensification of this zonal overturning circulation and the resulting cooling of the tropical eastern Pacific contributed to the pronounced slowdown in the rate of global warming that occurred around the beginning of the current millennium.

Despite the array of statistical and modeling evidence that has been presented in support of the role of the ocean in thermodynamic forcing, many climate scientists remain convinced that the irregularities in the rate of warming in the historical record are attributable to variations in the time-varying anthropogenic forcing by aerosols. For example, on the basis of numerical experiments with a state-of-the-art climate system model, Booth et al. (2012) conclude that aerosol emissions and periods of volcanic activity explain 76 per cent of the simulated multidecadal variance in detrended 1860–2005 North Atlantic sea surface temperatures and that after 1950, their simulated variability is within observational estimates. Numerical experiments reported in the attribution chapter of the IPCC’s Fourth Assessment Report (Hegerl et al. 2007) and highlighted in the Technical Summary also portray the late 20th Century warming in GST as being entirely in response to anthropogenic forcing. For further discussion of these issues see Zhang et al. (2013) and Chapters XX, XX, XX, and XX of this book.

Another arena in which thermodynamically forced internal variability of the climate system might come into play is through the feedbacks associated with the fluxes of latent and sensible heat by soil moisture and vegetation during the warm season (or in the tropics, during the growing season). Although land surface processes act on rather short time scales, the existence of positive feedbacks can serve to amplify the variability on all time scales. Another aspect of this problem on a regional scale is the existence of human-induced external forcings not directly related to global warming; *e.g.*, cultivation, irrigation, deforestation and afforestation, and inadvertent desertification.

5. Summary and Discussion

In this chapter we have categorized SAT trends as being externally forced versus internally generated (*i.e.*, forced versus free) and as being dynamically versus thermodynamically induced, as elaborated in Fig. 1. The distinction between forced and free is illuminated by analysis of numerical simulations in which a single model is run with a single set of time dependent external forcings but starting from a suite of different atmospheric initial conditions, yielding an ensemble of time-dependent climate scenarios. The dynamically induced component of the SAT trend is isolated by linear regression using the SLP field as a “predictor” and the individual ensemble members as samples. When ensembles of climate scenarios are not available, the regression can be performed in the time domain. In principle, this methodology can be applied to variables other than SAT and variables other than SLP can be used as “predictors” of the dynamically-induced trends.

The relative importance of the forced and free components of the trends depends upon the interval τ over which the trends are computed. If the forced component can be viewed as increasing linearly with τ and the dynamically-induced variability can be modeled as white noise whose contribution to the variance of the trend is inversely proportional to τ , then the prominence of the forced component (*i.e.*, the ratio of the trend to the standard deviation of the variability about the trend) should vary as $\tau^{3/2}$. The “signal” in the SAT trends is also latitude dependent (*i.e.*, much more prominent in the tropics than in the extratropics) and dependent upon the spatial averaging. Here we have focused mainly on SAT trends over the continental US within 36 and 56 year intervals. The individual ensemble members in

large ensembles of simulations are shown to exhibit a remarkable amount of diversity, most of which is dynamically induced. That this dynamical contribution to the variability is as large in an atmospheric model run with SST prescribed in accordance with its seasonally varying climatology as in the coupled runs suggests that the dynamically induced component of the trends is mainly attributable to atmosphere’s own internal variability rather than to coupled atmosphere-ocean interactions.

Whether the real climate system exhibits as much dynamically-induced variability as the climate models examined in this study remains to be determined. There are indications that the temporal variance of the atmospheric circulation in the CAM3 is somewhat overestimated (Deser et al. 2012a) and this may also be true of CCSM4. If this is the case, one might expect the dynamically-induced variability to be overestimated as well. On the other hand, it is possible that the coupled atmosphere-ocean system exhibits multidecadal variability that is not fully captured by the models (Deser et al. 2012c; Danabasoglu et al. 2012), in which case, the uncertainty inherent in projections of 56-year SAT trends might be underestimated.

Dynamically-induced atmospheric variability accounts for ~ 0.7 of the 1.7°C the warming of the Northern Hemisphere continents from 1965 to 2000, but this has had only a small effect on the globally averaged warming. A potentially more important contributor to multidecadal variations in the rate of rise of GST is the variability in the strength of the MOC, which modulates the fluxes of sensible and latent heat at the air-sea interface over the subpolar North Atlantic and parts of the Arctic. Just how much of the spatial and temporal variability in the rate of warming over the con-

tinents is MOC-related how much of it is induced by spatial and temporal inhomogeneities in the forcing by greenhouse gases and aerosols has important implications for estimates of climate sensitivity. If the enhanced late 20th century warming was, indeed, a reflection of the internal variability of the climate system, the climate models purported to replicate it in ensemble-mean simulations may be getting the right answer for the wrong reason; i.e., they may be overly sensitive to the radiative forcing.

We have shown that sampling variability constitutes a large part of the uncertainty inherent in projections of regional climate change over the next 50 years, even in averages over areas as large as the continental US. The uncertainty in estimates of the forced response can be narrowed by performing ensembles of simulations and/or by applying dynamical adjustments to the individual ensemble members. However, even if the forced variability were known exactly, the inherently unpredictable, internally generated sampling variability in the future trajectory of the climate system would still remain because it is only one member of an ensemble of possible time-dependent scenarios that could result from a single prescribed external forcing. During the summer season the internally generated SLP variability is smaller than during winter but the thermodynamic consequences of changing atmospheric circulation patterns could be amplified by hydrologic and terrestrial biosphere feedbacks. Deterministic, multidecadal, MOC-related variability is an additional source of uncertainty that could modulate or even temporarily reverse the sign of short term GST trends, as discussed in Chapter XX.

The large sampling variability inherent in local or regional interdecadal and multidecadal temperature trends has implications for the attribution of record high temperature events and heat waves, whose frequency of occurrence is closely tied to the mean temperature (Wergen and Krug 2010; Lau and Nath 2012, Coumou et al. 2013). To the extent that inherently stochastic trends in atmospheric circulation patterns modulate local seasonal mean temperatures, they also raise or lower the frequency of occurrence of extreme events, resulting in clusters of extreme events in particular geographical “hot spots” while extreme event statistics other regions may appear to be unaffected by climate change.

Opponents of environmental protection exploit the uncertainties inherent in projections of future climate change to cast doubt on the immediacy, seriousness, and policy relevance of human-induced environmental degradation and to portray the scientific community as “crying wolf.” The sampling issues discussed in this chapter afford the so-called “climate skeptics” some degree of aid and comfort, but not nearly as much as they derive from misstatements about attribution of extreme events and exaggerated projections of regional, near term climate change. Until the signal of human-induced climate change emerges more clearly above background variability, a more compelling case for environmental protection, including reductions the emissions of greenhouse gases, can be made by focusing on the impacts of human-induced warming in the tropics, where the “signal to noise ratio” is much stronger (Mahlstein et al. 2011, 2012) and on the combined impacts of climate change, looming shortages of fresh water (Pearce 2007; Brown 2010) and loss of topsoil (Montgomery 2009) on food security.

References

- Alekseev, V. A., P. L. Langen, and J. R. Bates, 2005: Polar amplification of surface warming on an aquaplanet in “ghost forcing” experiments without sea ice feedbacks. *Clim. Dyn.*, **24**, 655–666.
- Álvarez-García, F., M. Latif, and A. Biastoch, 2008: On Multidecadal and Quasi-Decadal North Atlantic Variability. *J. Climate*, **21**, 3433–3452.
- Barnett, T., F. Zwiers, G. Hegerl, M. Allen, T. Crowley, N. Gillett, K. Hasselmann, P. Jones, B. Santer, R. Schnur, P. Stott, K. Taylor and S. Tett, 2005: Detecting and attributing external influences on the climate system: a review of recent advances. *J. Climate*, **18**, 1291–1314.
- Black, E., M. Blackburn, G. Harrison, B. J. Hoskins and J. Methven, 2004: Factors contributing to the summer 2003 European heatwave, *Weather*, **59**, 217–223.
- B. B. Booth, N. J. Dunstone, P. R. Halloran, T. Andrews, N. Bellouin, 2012: Aerosols implicated as a prime driver in twentieth century North Atlantic climate variability, *Nature*, **484**, 228–232.
- Bracco, A., F. Kucharski, R. Kallumal and F. Molteni, 2004: Internal variability, external forcing and climate trends in multi-decadal AGCM ensembles. *Clim. Dyn.*, **23**, 659–678.
- Brown, L. R., 2011: *World on Edge: How to Prevent Economic and Environmental Collapse*, W. W. Norton Co., 240 pp.
- Chiang, J. C. H., and A. Sobel, 2002: Tropical tropospheric temperature variations caused by ENSO and their influence on the remote tropical climate. *J. Climate*, **15**, 2616–2631.
- Clement, A., P. DiNezio, and C. Deser, 2011: Rethinking the Ocean’s Role in the Southern Oscillation, *J. Climate*, **24**, 4056–4072.
- Compo, G. P., and Coauthors, 2011: The Twentieth Century Reanalysis Project. *Quart. J. Roy. Meteorol. Soc.*, **137**, 1–28.
- Coumou, D., A. Robinson, and S. Rahmstorf, 2013: Global increase in record-breaking monthly-mean temperatures. *Climatic Change*, doi:10.1007/s10584-012-0668-1.
- Danabasoglu, G., S. G. Yeager, Y.-Oh Kwon, J. J. Tribbia, A. S. Phillips, and J. W. Hurrell, 2012: Variability of the Atlantic Meridional Overturning Circulation in CCSM4. *J. Climate*, **25**, 5153–5172.
- DelSole, T., M. K. Tippett, and J. Shukla, 2011: A significant component of unforced multidecadal variability in the recent acceleration of global warming. *J. Climate*, **24**, 909–926.
- Deser, C., A. S. Phillips, M. Alexander and B. V. Smoliak, 2013: Projecting North American Climate Over the Next 50 Years: Uncertainty due to Internal Variability. *J. Climate*, submitted.
- Deser, C., A. S. Phillips, V. Bourdette, and H. Teng, 2012a: Uncertainty in climate change projections: The role of internal variability. *Clim. Dyn.*, **38**, 527–546.
- Deser, C., R. Knutti, S. Solomon, and A. S. Phillips, 2012b: Communication of the role of natural variability in future North American climate. *Nature: Climate Change*, **2**, 775–779.
- Deser, C., A. S. Phillips, R. A. Tomas, Y. Okumura, M. A. Alexander, A. Capotondi, J. D. Scott, Y.-O. Kwon, and M. Ohba, 2012c: ENSO and Pacific decadal variability in Community Climate System Model Version 4. *J. Climate*, **25**, 2622–2651.
- Deser, C., and A. S. Phillips, 2009: Atmospheric circulation trends, 1950–2000: The relative roles of sea surface temperature forcing and direct atmospheric radiative forcing. *J. Climate*, **22**, 396–413.
- Dole, R., M. P. Hoerling, J. Perlwitz, J. Eischeid, P. Pegion, T. Zhang, X. -W. Quan, T. Xu, and D. Murray, 2012: Was there a basis for anticipating the 2011 Russian heat wave? *Geophys. Res. Lett.*, **38**, L06702.
- Dommenget, D., 2010: The slab ocean El Niño, *Geophys. Res. Lett.* **37**, L20701.
- Gent, P. R., and Coauthors, 2011: The Community Climate System Model version 4. *J. Climate*, **24**, 4973–4991.
- Gillett, N. P., and D. W. J. Thompson, 2003: Simulation of recent Southern Hemisphere climate change. *Science*, **302**, 273–275.
- Gulev, S. K., M. Latif, N. Keenlyside, W. Park, and K. P. Koltermann, 2013: North Atlantic Ocean control on surface heat flux on multidecadal timescales, *Nature*, **499**, 464–467.
- Hartmann, D. L., J. M. Wallace, V. Limpasuvan, D. W. J. Thompson and J. R. Holton, 2000: Can ozone depletion and global warming interact to produce rapid climate change? *Proc. Nat. Acad. Sci.*, **97**, 1412–1417.
- Hegerl, G. C., and Coauthors, 2007: Understanding and attributing climate change. *Climate Change 2007: The Physical Science Basis. Contribution of Working Group I to the Fourth Assessment Report of the IPCC*, Solomon, S., et al., Eds., Cambridge University Press, Cambridge, 663–745.
- Held, I. M., and B. J. Soden, 2006: Robust responses of

- the hydrological cycle to global warming. *J. Climate*, **19**, 5686–5699.
- Hu, Z.-Z., A. Kumar, H.-L. Ren, H. Wang, M. L'Heureux, F.-F. Jin, 2013: Weakened Interannual Variability in the Tropical Pacific Ocean since 2000, *J. Climate*, **26**, 2601–2613.
- Hurrell, J. W., 1996: Influence of variations in extratropical wintertime teleconnections on Northern Hemisphere temperature. *Geophys. Res. Lett.*, **23**, 665–668.
- Kitoh, A., T. Motoi, and H. Koide, 1999: SST variability and its mechanism in a coupled atmosphere-mixed layer ocean model, *J. Climate*, **12**, 1221–1239.
- Kosaka, Y., and S.-P. Xie, 2013: Recent global-warming hiatus tied to equatorial Pacific surface cooling, *Nature*, doi: 10.1038/nature12534.
- Kutzbach, J. E., 1981: Monsoon climate of the Early Holocene: Climate experiment with the Earth's orbital parameters for 9000 years ago. *Science*, **214**, 59–61.
- Lau, N.-C., M. J. Nath, 2012: A Model Study of Heat Waves over North America: Meteorological Aspects and Projections for the Twenty-First Century. *J. Climate*, **25**, 4761–4784.
- Lu, J., G. A. Vecchi, and T. Reichler, 2007: Expansion of the Hadley cell under global warming. *Geophys. Res. Lett.*, **34**, L06805.
- Madden, R. A., and J. Williams, 1978: The Correlation between Temperature and Precipitation in the United States and Europe. *Mon. Wea. Rev.*, **106**, 142–147.
- Mahlstein, I., G. Hegerl, and S. Solomon, 2012: Emerging local warming signals in observational data. *Geophys. Res. Lett.*, **39**, L21711.
- Mahlstein, I., R. Knutti, S. Solomon, and R. W. Portmann, 2011: Early onset of significant local warming in low latitude countries. *Environ. Res. Lett.*, **6**, 034009.
- Mantua, N. J., S. R. Hare, Y. Zhang, J. M. Wallace, and R. C. Francis, 1997: An interdecadal oscillation with impacts on salmon production. *Bull. Amer. Meteor. Soc.*, **78**, 1069–1079.
- Meehl, G. A., A. Hu, J. Arblaster, J. Fasullo and K. E. Trenberth, 2013: Externally forced and internally generated decadal climate variability associated with the Interdecadal Pacific Oscillation. *J. Climate*, *in press*.
- Meehl, G. A., J. M. Arblaster, J. T. Fasullo, A. Hu, and K. E. Trenberth, 2011: Model-based evidence of deep-ocean heat uptake during surface-temperature hiatus periods, *Nature Climate Change*, **1**, 360–364.
- Meehl, G. A., and Coauthors, 2007: Global Climate Projections. *Climate Change 2007: The Physical Science Basis. Contribution of Working Group I to the Fourth Assessment Report of the IPCC*, Solomon, S., et al., Eds., Cambridge University Press, 747–845.
- Miller, R. L., G. A. Schmidt, and D. T. Shindell, 2006: Forced annular variations in the 20th century Intergovernmental Panel on Climate Change Fourth Assessment Report models. *J. Geophys. Res.*, **111**, D18101.
- Montgomery, D. R., *Dirt: The Erosion of Civilizations*, University of California Press, 295 pp.
- Newman, M., G. P. Compo and M. A. Alexander, 2003: ENSO-forced Variability of the Pacific Decadal Oscillation, *J. Climate*, **16**, 3853–3857.
- Nitta, T. and S. Yamada, 1989: Recent warming of tropical sea surface temperature and its relationship to the Northern Hemisphere circulation. *J. Meteor. Soc. Japan*, **67**, 187–193.
- Oshima, K., Y. Tanimoto, and S.-P. Xie, 2012: Regional Patterns of Wintertime SLP Change over the North Pacific and Their Uncertainty in CMIP3 Multi-Model Projections, *J. Met. Soc. Japan*, **90A**, 385–396.
- Pearce, F., 2007: *When the Rivers Run Dry: Water, the Defining Crisis of the 21st Century*, Beacon Press, 336 pp.
- Polvani, L., D. Waugh, G. J. -P. Correa, and S.-W. Son, 2011: Stratospheric ozone depletion: The main driver of 20th century atmospheric circulation changes in the Southern Hemisphere. *J. Climate*, **24**, 795–812.
- Randall, D.A., and Coauthors, 2007: Climate models and their evaluation. *Climate Change 2007: The Physical Science Basis. Contribution of Working Group I to the Fourth Assessment Report of the IPCC*, Solomon, S., et al., Eds., Cambridge University Press, 589–662.
- Robock, A., and J. Mao, 1994: The volcanic signal in surface temperature observations. *J. Climate*, **8**, 1086–1103.
- Semenov, V. A., M. Latif, D. Dommenget, N. S. Keenlyside, A. Strehz, T. Martin and W. Park, 2010: The impact of North Atlantic-Arctic multidecadal variability on Northern Hemisphere surface air temperature. *J. Climate*, **23**, 5668–5677.
- Shindell, D. T., G. A. Schmidt, R. L. Miller, D. Rind, 2001: Northern Hemisphere winter climate response to greenhouse gas, ozone, solar, and volcanic forcing. *J. Geophys. Res.*, **106**, 7193–7210.
- Smoliak, B. V., J. M. Wallace, M. T. Stoelinga and T. P. Mitchell, 2010: Application of partial least squares regression to the diagnosis of year-to-year variations in Pacific Northwest snowpack and Atlantic hurricanes. *Geophys. Res. Lett.*, **37**, L03801.

- Solomon, S., and Coauthors, 2007: Technical Summary. *Climate Change 2007: The Physical Science Basis. Contribution of Working Group I to the Fourth Assessment Report of the IPCC*, Solomon, S., et al., Eds. Cambridge University Press, 63pp.
- Thompson, D. W. J., and S. Solomon, 2002: Interpretation of recent Southern Hemisphere climate change. *Science*, **296**, 895–899.
- Thompson, D. W. J., and J. M. Wallace, 2000: Annular modes in the extratropical circulation. Part 1: month-to-month variability. *J. Climate*, **13**, 1000–1016.
- Thompson, D. W. J., J. M. Wallace, P. D. Jones and J. J. Kennedy, 2009: Identifying signatures of natural climate variability in time series of global mean surface temperature: methodology and insights. *J. Climate*, **22**, 6120–6141.
- Trenberth, K. E., and Coauthors, 2007: Observations: Surface and Atmospheric Climate Change. *Climate Change 2007: The Physical Science Basis. Contribution of Working Group I to the Fourth Assessment Report of the IPCC*, Solomon, S., et al., Eds., Cambridge University Press, 235–335.
- Trenberth, K. E., and D. J. Shea, 2005: Relationships between precipitation and surface temperature. *Geophys. Res. Lett.*, **32**, L14703.
- Trenberth, K. E., and T. J. Hoar, 1997: El Niño and climate change. *Geophys. Res. Lett.*, **24**, 3057–3060.
- Trenberth, K. E., and T. J. Hoar, 1996: The 1990–1995 El Niño–Southern Oscillation Event: Longest on Record. *Geophys. Res. Lett.*, **23**, 57–60.
- Trenberth, K. E., and J. W. Hurrell, 1994: Recent observed interdecadal climate changes in the Northern Hemisphere. *Bull. Amer. Meteorol. Soc.*, **71**, 988–993.
- Vecchi, G. A., and B. J. Soden, 2007: Global warming and the weakening of the tropical circulation. *J. Climate*, **20**, 4316–4340.
- Wallace, J. M., Q. Fu, B. V. Smoliak, P. Lin, and C. M. Johanson, 2012: Simulated versus observed patterns of warming over the extratropical Northern Hemisphere continents during the cold season. *Proc. Natl. Acad. Sci.*, **109**, 14337–14332.
- Wallace, J. M., and D. W. J. Thompson, 2002: Annular modes and climate prediction. *Physics Today*, **55**, 28–33.
- Wallace, J. M., Y. Zhang, and L. Bajuk, 1996: Interpretation of Interdecadal Trends in Northern Hemisphere Surface Air Temperature. *J. Climate*, **9**, 249–259.
- Wallace, J. M., Y. Zhang, and J. A. Renwick, 1995: Dynamic contribution to hemispheric mean temperature trends. *Science*, **270**, 780–783.
- Wergen, G. and J. Krug, 2010: Record breaking temperatures reveal a warming climate. *Europhysics Lett.*, **92**, 30008.
- Wu, Z., N. E. Huang, J. M. Wallace, B. V. Smoliak, and X. Chen, 2011: On the time-varying trend in global-mean surface temperature. *Clim. Dyn.*, **37**, 759–773.
- Yin, J. H., 2005: A Consistent poleward shift of the storm tracks in simulations of 21st Century climate. *Geophys. Res. Lett.*, **32**, L18701.
- Yulaeva, E., and J. M. Wallace, 1994: The signature of ENSO in global temperature and precipitation fields derived from the microwave sounding unit. *J. Climate*, **7**, 1719–1736.
- Zhang, R., T. L. Delworth, R. Sutton, D. Hodson, K. Dixon, I. M. Held, Y. Kushnir, J. Marshall, Y. Ming, R. Msadek, J. Robson, T. Rosati, M. Ting, G. Vecchi, 2013: Have Aerosols Caused the Observed Atlantic Multi-decadal Variability? *J. Atmos. Sci.*, **70**, 1135–1144.
- Zhang, Y., J. M. Wallace and D. S. Battisti, 1997: ENSO-like interdecadal variability: 1900–1993. *J. Climate*, **10**, 1004–1020.